The high order variable-coefficient explicit-implicit-null method for diffusion and dispersion equations

Meiqi Tan[1], Juan Cheng[2], and Chi-Wang Shu[3]

Abstract

For the high order diffusion and dispersion equations, the general practice of the explicit-implicit-null (EIN) method is to add and subtract an appropriately large linear highest derivative term with constant coefficient at one side of the equation, and then apply the standard implicit-explicit method to the equivalent equation. We call this approach the constant-coefficient EIN method in this paper and hereafter denote it by "CC-EIN". To reduce the error in the CC-EIN method, the variable-coefficient explicit-implicit-null (VC-EIN) method, which is obtained by adding and subtracting a linear highest derivative term with variable coefficient, is proposed and studied in this paper. Coupled with the local discontinuous Galerkin (LDG) spatial discretization, the VC-EIN method is shown to be unconditionally stable and can achieve high order of accuracy for both one-dimensional and two-dimensional quasi-linear and nonlinear equations. In addition, although the computational cost slightly increases, the VC-EIN method can obtain more accurate results than the CC-EIN method, if the diffusion coefficient or the dispersion coefficient has a few high and narrow bumps and the bumps only account for a small part of the whole computational domain.

Keywords: diffusion equation, dispersion equation, stability, explicit-implicit-null time discretization, local discontinuous Galerkin method.

[1] Graduate School, China Academy of Engineering Physics, Beijing 100088, China. E-mail: tanmeiqi20@gscaep.ac.cn.

[2] Corresponding author. Laboratory of Computational Physics, Institute of Applied Physics and Computational Mathematics, Beijing 100088, China and HEDPS, Center for Applied Physics and Technology, and College of Engineering, Peking University, Beijing 100871, China. E-mail: cheng_juan@iapcm.ac.cn. Research is supported in part by National Key R&D Program of China No. 2023YFA1009003, and NSFC grant 12031001.

[3] Division of Applied Mathematics, Brown University, Providence, RI 02912, USA. E-mail: chi-wang_shu@brown.edu. Research is supported in part by NSF grants DMS-2010107 and DMS-2309249.

1 Introduction

In this paper, we exploit a third order variable-coefficient explicit-implicit-null (VC-EIN) time-marching method coupled with the local discontinuous Galerkin (LDG) methods for solving high order diffusion and dispersion equations, respectively. For the simplification of notations, the equations described below are only one-dimensional. Note that the conclusions given in this paper can also be extended to equations in higher dimensions, and we shall present two-dimensional examples in the numerical experiment section.

The second order diffusion equation

$$U_t = (d(U)U_x)_x, \tag{1.1}$$

where the diffusion coefficient $d(U) \geq 0$ is smooth and bounded, has been widely used to model various processes in engineering and industry, such as the thermo-chemical diffusion process of carburizing and nitriding [5], the miscible displacement in porous media [21] and so on. In this paper, we use the capital letter U to denote the exact solution to the considered equation.

The dispersion equation

$$U_t + g(U_x)_{xx} = 0 \tag{1.2}$$

is a special KdV-type equation, which has been widely used to describe the propagation of waves in a variety of nonlinear dispersive media and appears often in applications. Applications include the study of waves in plasma physics, internal waves in coastal waters, flow in blood vessels and so on. For more details, we refer the readers to [3] and the references therein.

The fourth order diffusion equation

$$U_t + (d(U_x)U_{xx})_{xx} = 0 \tag{1.3}$$

is a special biharmonic-type equation, where the nonlinear term could be more general but we just present (1.3) as an example. The biharmonic-type equations have wide applications in thin plate bending theory, strain gradient elasticity, phase-field modelling and mathematical biology.

The explicit-implicit-null (EIN) method denotes an IMEX-type time-marching method for a problem of the form

$$\frac{\mathrm{d}u}{\mathrm{d}t} = f(t,u)$$

obtained by adding and subtracting an approximation $g(t,u)$ of the stiff terms in $f(t,u)$ which is more amenable for an implicit treatment

$$\frac{\mathrm{d}u}{\mathrm{d}t} = f(t,u) - g(t,u) + g(t,u),$$

and then applying the standard implicit-explicit (IMEX) method to the above equation. Namely, we treat the term $f(t,u)-g(t,u)$ explicitly and the remaining term $g(t,u)$ implicitly. Since the piece $g(t,u)$ that is added to the equation is then subtracted (seemingly adding zero), Duchemin and Eggers [9] proposed to call this approach the "explicit-implicit-null method", or EIN method for short. The crucial step to the success of the method consists in adding and subtracting the right term, which is quite flexible in the selection, but needs to have the same scaling in wave number as the stiffest term in the equation.

The EIN method, which was first introduced by Douglas and Dupont [8], has been applied on a case-by-case basis to, for example, the two models of motion by mean curvature and motion by surface diffusion [13], the Boltzmann equation near the fluid dynamic regime [10], the nonlinear hyperbolic systems containing fully nonlinear and stiff relaxation terms [4], the porous medium equation and the high-field model in semiconductor device simulations [16], the Navier-Stokes equations [11], the Cahn-Hilliard equations [12], the KdV-type equations [14, 15] and so on.

For the high order diffusion and dispersion equations studied in this paper, the general practice of the EIN method is to add and subtract an appropriately large linear highest derivative term with constant coefficient at one side of the equation, and then apply the IMEX time-marching method to the equivalent equation. We call such method the constant-coefficient explicit-implicit-null method in this paper and hereafter denote it by "CC-EIN".

In the following, we take the second order diffusion equation (1.1) as an example. Since the equation contains a stiff part corresponding to the second derivative, in order to stabilize the equation, a second derivative term with constant coefficient $b_1 U_{xx}$ is added to and subtracted from the left-hand side of the considered equation

$$U_t + \underbrace{b_1 U_{xx} - (d(U)U_x)_x}_{T_1} - \underbrace{b_1 U_{xx}}_{T_2} = 0, \qquad b_1 = a_0 \cdot \max d(u^n), \tag{1.4}$$

where u^n represents the numerical solution at the n-th time level. Here, a_0 is an appropriately large constant such that T_1 is either not stiff, or less stiff and less dissipative compared to T_2, thus it can be treated explicitly, and T_2 is stiff and dissipative, thus will be discretized implicitly. The CC-EIN method so designed has great flexibility in dealing with stiff nonlinear problems, as it gives rise to a linear system for which very efficient solution methods exist. In addition, the severe time step restriction imposed by the explicit treatment of the nonlinear stiff term $(d(U)U_x)_x$ can be removed. Since the auxiliary term $b_1 U_{xx}$ added to and subtracted from the equation are treated in different ways, i.e., one is treated explicitly and the other is treated implicitly, for a p-th order CC-EIN method, stabilization is achieved essentially at the cost of a somewhat additional temporal truncation error of order $O(\tau^p)$, where τ is the time step. When the dominant error is due to the time-stepping or the spatial order of accuracy is at least the same as that of the time-marching method, the numerical results in [14] show that the overall error will increase significantly with the increase of b_1 in (1.4). In such situation, if the diffusion coefficient $d(U)$ has a few high and narrow bumps and the bumps only account for a small part of the whole computational domain, the coefficient of the additional error $O(\tau^p)$ of the CC-EIN method is relatively large. To resolve this issue, the VC-EIN method, which has not been studied before to our knowledge, is proposed and studied in this paper.

The VC-EIN method is obtained by adding and subtracting a more accurate approximation of the stiffest term at one side of the equation, and then treating them separately. In the following, we still take the diffusion equation (1.1) as an example. From the stability and conservation points of view, we add and subtract a second derivative term with variable coefficient $(a_1(x)U_x)_x$ at the left-hand side of the considered equation

$$U_t - \underbrace{(d(U)U_x - a_1(x)U_x)_x}_{T_1} - \underbrace{(a_1(x)U_x)_x}_{T_2} = 0, \tag{1.5}$$

where

$$a_1(x) = a_0 \cdot \max_{t^n \le t \le t^{n+1}} d(u(x,t)),$$

and then treat the damping term T_2 implicitly and the remaining term T_1 explicitly. Similarly, the explicit treatment of T_1 and the implicit discretization of the linear term T_2 will lead to a linear system, which is relatively easy to solve by many direct or iterative methods. Compared to other methods that also do not require solving nonlinear equations, such as the Rosenbrock-type methods [2], our method is easier to implement. In addition, compared with the CC-EIN method, the additional error introduced by the different treatments of the auxiliary term $(a_1(x)U_x)_x$ in the VC-EIN method is smaller outside the bumps of $d(U)$. When the high and narrow bumps only account for a small part of the whole computational domain, the VC-EIN method will eventually lead to a smaller global error at least for the L^1 and L^2 norms, and much smaller errors locally away from the high bumps, see the numerical results in Section 3.

In relation to the spatial discretizations, we adopt the LDG method for the high order diffusion and dispersion equations, respectively. The LDG method, which was first introduced by Cockburn and Shu [6] for the convection-diffusion equations, has been popular. It can easily handle meshes with hanging nodes, elements of general shapes and local spaces of different types, thus it is flexible for *hp*-adaptivity. For the references on LDG methods as well as their implementation and applications, see the review paper by Cockburn and Shu [7]; see also the papers [17–20] (the list is far from being exhaustive). Since the stabilization of both of the EIN methods (VC-EIN and CC-EIN) is achieved essentially at the cost of a somewhat additional temporal error, the specific choice of spatial discretization does not have much impact on the effectiveness of the VC-EIN method in reducing such error.

Therefore, we can also consider other spatial discretizations such as the finite difference, the finite volume and the spectral methods.

An outline of this paper is as follows. In Section 2, we will present the semi-discrete LDG schemes and the time discretization method for the equations mentioned above. In addition, we will propose a guidance for the choices of $a_1(x)$ to ensure the stability of the VC-EIN-LDG schemes. Section 3 shows a series of numerical examples to test the stability and error accuracy of the proposed schemes for both one-dimensional and two-dimensional quasi-linear and nonlinear problems. In addition, we will also carry out a comparative study about the numerical performance of the VC-EIN-LDG scheme and the CC-EIN method with LDG spatial discretization (CC-EIN-LDG). When proper parameters are chosen, the numerical results show that the VC-EIN-LDG scheme can outperform the CC-EIN-LDG scheme, especially for local errors outside the bumps. Finally, the concluding remarks are given in Section 4.

2 The numerical schemes

In this section, we will present the semi-discrete LDG schemes and the time discretization method used in this paper. In addition, we will propose a guidance for the choices of $a_1(x)$ to ensure the stability of the VC-EIN-LDG schemes. For simplicity of presentation, some preliminary notations are presented here. Let $\mathcal{T}_h = \{I_j = [x_{j-\frac{1}{2}}, x_{j+\frac{1}{2}}]\}_{j=1}^{N}$ be a uniform partition of the computational domain $\Omega = [x_L, x_R]$, where $x_{\frac{1}{2}} = x_L$ and $x_{N+\frac{1}{2}} = x_R$ are the two boundary endpoints. The spatial mesh size is $h = (x_R - x_L)/N$.

2.1 The LDG method for the second order diffusion equation

Let us describe in detail the implementation of the LDG method for the second order diffusion equation (1.5) subject to periodic boundary condition and the initial condition

$$U(x,0) = U_0(x), \qquad x \in \Omega. \tag{2.1}$$

Note that the LDG method described in this paper is slightly different from the classical one [7] which involves the square root of the diffusion coefficient $d(U)$. The idea of the LDG method is to rewrite the equation with higher order derivatives into an equivalent first order system, and then apply the discontinuous Galerkin (DG) method [7] to the system, so the LDG scheme shares the advantages of the DG method. To define the LDG method, we first introduce the new variables

$$P = (d(U) - a_1(x))R, \qquad Q = a_1(x)R, \qquad R = U_x,$$

and reformulate (1.5) as the following first order system

$$\begin{aligned} U_t - P_x - Q_x &= 0, & P - (d(U) - a_1(x))R &= 0, \\ Q - a_1(x)R &= 0, & R - U_x &= 0. \end{aligned}$$

Then we seek piecewise polynomial solutions u, p, q, r from V_h such that for all the test functions ϕ_1, ϕ_2, ϕ_3, $\phi_4 \in V_h$ and $1 \le j \le N$, we have

$$\int_{I_j} u_t\phi_1 \, \mathrm{d}x + \int_{I_j} (p+q)(\phi_1)_x \, \mathrm{d}x - (\hat{p}+\hat{q})_{j+\frac{1}{2}}(\phi_1)^-_{j+\frac{1}{2}} + (\hat{p}+\hat{q})_{j-\frac{1}{2}}(\phi_1)^+_{j-\frac{1}{2}} = 0, \tag{2.2a}$$

$$\int_{I_j} p\phi_2 \, \mathrm{d}x = \int_{I_j} (d(u) - a_1(x))r\phi_2 \, \mathrm{d}x, \tag{2.2b}$$

$$\int_{I_j} q\phi_3 \, \mathrm{d}x = \int_{I_j} a_1(x)r\phi_3 \, \mathrm{d}x, \tag{2.2c}$$

$$\int_{I_j} r\phi_4 \, \mathrm{d}x + \int_{I_j} u(\phi_4)_x \, \mathrm{d}x - \hat{u}_{j+\frac{1}{2}}(\phi_4)^-_{j+\frac{1}{2}} + \hat{u}_{j-\frac{1}{2}}(\phi_4)^+_{j-\frac{1}{2}} = 0 \tag{2.2d}$$

and

$$u(x,0) = \mathbb{P}_h U_0(x), \tag{2.3}$$

where

$$V_h = \{\phi \in L^2(\Omega) : \phi|_{I_j} \in \mathcal{P}_k(I_j), \, \forall j = 1, ..., N\} \tag{2.4}$$

and $\mathbb{P}_h U_0(x)$ is the local L^2-projection of the initial condition $U_0(x)$ satisfying

$$\int_{I_j} \mathbb{P}_h U_0(x)\phi_1(x) \, \mathrm{d}x = \int_{I_j} U_0(x)\phi_1(x) \, \mathrm{d}x, \qquad \forall \phi_1(x) \in V_h. \tag{2.5}$$

Here, $\mathcal{P}_k(I_j)$ is the space of polynomials in cell I_j of degree no more than k. The functions in V_h are allowed to have discontinuities across cell interfaces. For any piecewise function u in V_h, we denote by $u^-_{j+\frac{1}{2}}$ and $u^+_{j+\frac{1}{2}}$ the left and right limits of the discontinuous solution u at the interface $x_{j+\frac{1}{2}}$, respectively. Now, the only ambiguity in the algorithm (2.2) is the definition of the numerical fluxes (the terms with the "hat"), which are single-valued functions defined at the interfaces and play important roles in ensuring stability of the LDG method. As shown in Section A.1 in Appendix, we can prove a strong L^2-stability result if we adopt the following numerical fluxes

$$\hat{p} = p^+, \qquad \hat{q} = q^+, \qquad \hat{u} = u^-, \tag{2.6}$$

where we have omitted the subscripts $j \pm \frac{1}{2}$ in the definition of the fluxes, as all quantities are evaluated at the interfaces $x_{j\pm\frac{1}{2}}$. We remark that the choice of the fluxes is not unique. In fact the crucial part is taking $\hat{p}$ and $\hat{q}$ from the same side and taking $\hat{u}$ and $\hat{p}$ from opposite sides (alternating fluxes). Note that we only need to replace the above-mentioned $a_1(x)$ with b_1 to obtain the LDG spatial discretization of the equation (1.4).

2.2 The LDG method for the dispersion equation

Since the dispersion equation (1.2) contains a stiff part corresponding to the third derivative, in order to stabilize the equation without sacrificing the conservation of the numerical solution, we add the same term $(a_1(x)U_x)_{xx}$, $a_1(x) \geq 0$ to both sides of the equation. It should be noted that the sign of the auxiliary term $(a_1(x)U_x)_{xx}$ we add to both sides of the equation needs to be adjusted according to the sign of $g'(U_x)$. If $g'(U_x) \geq 0$ within the whole computational domain Ω, we should add two equal term with negative prefix $-(a_1(x)U_x)_{xx}$ to both sides of the considered equation. Otherwise, the sign of the auxiliary term $(a_1(x)U_x)_{xx}$ needs to be positive. We only consider the case where the sign of $g'(U_x)$ is fixed. The discussion of the dispersion equation with the sign of $g'(U_x)$ varying in space and time goes beyond the scope of the present paper and is by itself an interesting topic for future investigation. Assuming that $g'(U_x) \geq 0$, we add two equal dispersion terms with variable coefficient $-(a_1(x)U_x)_{xx}$ to both sides of the equation and get

$$U_t + \underbrace{(g(U_x) - a_1(x)U_x)_{xx}}_{T_1} = -\underbrace{(a_1(x)U_x)_{xx}}_{T_2}, \tag{2.7}$$

where

$$a_1(x) = a_0 \cdot \max_{t^n \leq t \leq t^{n+1}} g'(u_x(x,t))$$

and $a_0 > 0$ is an appropriately large constant yet to be determined. We begin with the equation (2.7) to describe the LDG method. For a detailed introduction of the method, we refer the readers to [19].

By introducing the new variables

$$V = (g(Z) - a_1(x)Z)_x, \qquad W = (a_1(x)Z)_x, \qquad Z = U_x,$$

we can rewrite (2.7) into the following first order system

$$\begin{aligned} U_t + V_x + W_x &= 0, & V - (g(Z) - a_1(x)Z)_x &= 0, \\ W - (a_1(x)Z)_x &= 0, & Z - U_x &= 0. \end{aligned}$$

The semi-discrete LDG approximation to the dispersion equation (2.7) with the initial condition (2.1) and periodic boundary condition can be defined as follows: seek piecewise polynomial solutions u, v, w, z from V_h such that for all the test functions ϕ_1, ϕ_2, ϕ_3, $\phi_4 \in V_h$ and $1 \leq j \leq N$, we have

$$\int_{I_j} u_t\phi_1 \,\mathrm{d}x - \int_{I_j} (v+w)(\phi_1)_x \,\mathrm{d}x + (\hat{v}+\hat{w})_{j+\frac{1}{2}}(\phi_1)^-_{j+\frac{1}{2}} - (\hat{v}+\hat{w})_{j-\frac{1}{2}}(\phi_1)^+_{j-\frac{1}{2}} = 0, \tag{2.8a}$$

$$\begin{aligned} &\int_{I_j} v\phi_2 \,\mathrm{d}x + \int_{I_j} (g(z) - a_1(x)z)(\phi_2)_x \,\mathrm{d}x - \\ &(\hat{g} - \widehat{a_1 z})_{j+\frac{1}{2}}(\phi_2)^-_{j+\frac{1}{2}} + (\hat{g} - \widehat{a_1 z})_{j-\frac{1}{2}}(\phi_2)^+_{j-\frac{1}{2}} = 0, \end{aligned} \tag{2.8b}$$

$$\int_{I_j} w\phi_3 \,\mathrm{d}x + \int_{I_j} a_1(x)z(\phi_3)_x \,\mathrm{d}x - (\widehat{a_1 z})_{j+\frac{1}{2}}(\phi_3)^-_{j+\frac{1}{2}} + (\widehat{a_1 z})_{j-\frac{1}{2}}(\phi_3)^+_{j-\frac{1}{2}} = 0, \tag{2.8c}$$

$$\int_{I_j} z\phi_4 \,\mathrm{d}x + \int_{I_j} u(\phi_4)_x \,\mathrm{d}x - \hat{u}_{j+\frac{1}{2}}(\phi_4)^-_{j+\frac{1}{2}} + \hat{u}_{j-\frac{1}{2}}(\phi_4)^+_{j-\frac{1}{2}} = 0 \tag{2.8d}$$

and the equality (2.3) as the initial condition. Here, V_h is defined by (2.4). As shown in [19], we can prove an L^2-stability result, a cell entropy inequality for a more general case and obtain optimal error estimates for the linear case, if we adopt the following numerical fluxes

$$\hat{v} = v^+, \qquad \hat{w} = w^+, \qquad \hat{u} = u^-, \qquad \hat{g} = g(z^+), \qquad \widehat{a_1 z} = (a_1 z)^+. \tag{2.9}$$

We remark that the choice of the numerical fluxes $\hat{g}$ and $\widehat{a_1 z}$ is based on the assumption that $g'(U_x) \geq 0$. If $g'(U_x) \leq 0$, we should take $\hat{g} = g(z^-)$, $\widehat{a_1 z} = (a_1 z)^-$. Similarly, we only need to replace the above-mentioned $a_1(x)$ with b_1 to obtain the LDG spatial discretization of the equation

$$U_t + \underbrace{(g(U_x) - b_1 U_x)_{xx}}_{T_1} = \underbrace{-b_1 U_{xxx}}_{T_2}, \tag{2.10}$$

where $b_1 = a_0 \cdot \max g'(u_x(x, t^n))$ and $g'(U_x) \geq 0$.

2.3 The LDG method for the fourth order diffusion equation

Adding and subtracting a fourth derivative term with variable coefficient $(a_1(x)U_{xx})_{xx}$ at the left-hand side of the equation (1.3), we obtain

$$U_t + \underbrace{(d(U_x)U_{xx})_{xx} - (a_1(x)U_{xx})_{xx}}_{T_1} + \underbrace{(a_1(x)U_{xx})_{xx}}_{T_2} = 0, \tag{2.11}$$

where

$$a_1(x) = a_0 \cdot \max_{t^n \leq t \leq t^{n+1}} d(u_x(x,t)),$$

and $a_0 > 0$ is an appropriately large constant yet to be determined. We begin with the equation (2.11) to describe the LDG method. The LDG method described in this paper is slightly different from the classical one [20] which involves the square root of the diffusion coefficient $d(U_x)$. To define the LDG method, we introduce the new variables

$$V = U_x, \qquad W = V_x, \qquad P = (d(V) - a_1(x))W,$$

$$Q = a_1(x)W, \qquad R = P_x, \qquad Z = Q_x$$

and rewrite the equation (2.11) as a first order system

$$U_t + R_x + Z_x = 0, \qquad R - P_x = 0, \qquad Z - Q_x = 0,$$

$$P - (d(V) - a_1(x))W = 0, \qquad Q - a_1(x)W = 0, \qquad W - V_x = 0, \qquad V - U_x = 0.$$

The semi-discrete LDG approximation to (2.11) with the initial condition (2.1) and periodic boundary condition can be defined as follows: find u, v, w, p, q, r, $z \in V_h$ such that, for all the test functions $\phi_l \in V_h$, $1 \le l \le 7$ and $1 \le j \le N$ we have

$$\int_{I_j} u_t\phi_1 \,\mathrm{d}x - \int_{I_j} (r+z)(\phi_1)_x \,\mathrm{d}x + (\hat{r}+\hat{z})_{j+\frac{1}{2}}(\phi_1)^-_{j+\frac{1}{2}} - (\hat{r}+\hat{z})_{j-\frac{1}{2}}(\phi_1)^+_{j-\frac{1}{2}} = 0, \tag{2.12a}$$

$$\int_{I_j} r\phi_2 \,\mathrm{d}x + \int_{I_j} p(\phi_2)_x \,\mathrm{d}x - \hat{p}_{j+\frac{1}{2}}(\phi_2)^-_{j+\frac{1}{2}} + \hat{p}_{j-\frac{1}{2}}(\phi_2)^+_{j-\frac{1}{2}} = 0, \tag{2.12b}$$

$$\int_{I_j} z\phi_3 \,\mathrm{d}x + \int_{I_j} q(\phi_3)_x \,\mathrm{d}x - \hat{q}_{j+\frac{1}{2}}(\phi_3)^-_{j+\frac{1}{2}} + \hat{q}_{j-\frac{1}{2}}(\phi_3)^+_{j-\frac{1}{2}} = 0, \tag{2.12c}$$

$$\int_{I_j} p\phi_4 \,\mathrm{d}x = \int_{I_j} (d(v) - a_1(x))w\phi_4 \,\mathrm{d}x, \tag{2.12d}$$

$$\int_{I_j} q\phi_5 \,\mathrm{d}x = \int_{I_j} a_1(x)w\phi_5 \,\mathrm{d}x, \tag{2.12e}$$

$$\int_{I_j} w\phi_6 \,\mathrm{d}x + \int_{I_j} v(\phi_6)_x \,\mathrm{d}x - \hat{v}_{j+\frac{1}{2}}(\phi_6)^-_{j+\frac{1}{2}} + \hat{v}_{j-\frac{1}{2}}(\phi_6)^+_{j-\frac{1}{2}} = 0, \tag{2.12f}$$

$$\int_{I_j} v\phi_7 \,\mathrm{d}x + \int_{I_j} u(\phi_7)_x \,\mathrm{d}x - \hat{u}_{j+\frac{1}{2}}(\phi_7)^-_{j+\frac{1}{2}} + \hat{u}_{j-\frac{1}{2}}(\phi_7)^+_{j-\frac{1}{2}} = 0. \tag{2.12g}$$

As shown in Section A.2 in Appendix, we can prove a strong L^2-stability result if we adopt the following numerical fluxes

$$\hat{u} = u^+, \qquad \hat{v} = v^-, \qquad \hat{q} = q^+, \tag{2.13a}$$

$$\hat{p} = p^+, \qquad \hat{r} = r^-, \qquad \hat{z} = z^-. \tag{2.13b}$$

We remark that the choice of the fluxes is not unique. In fact the crucial part is taking $\hat{p}$ and $\hat{q}$ ($\hat{r}$ and $\hat{z}$) from the same side and taking $\hat{u}$ and $\hat{r}$ ($\hat{v}$ and $\hat{p}$) from opposite sides. Similarly, we only need to replace the above-mentioned $a_1(x)$ with b_1 to obtain the LDG spatial discretization of the equation

$$U_t + \underbrace{(d(U_x)U_{xx} - b_1U_{xx})_{xx}}_{T_1} + \underbrace{b_1U_{xxxx}}_{T_2} = 0, \tag{2.14}$$

where $b_1 = a_0 \cdot \max d(u_x(x,t^n))$ and $d(U_x) \ge 0$.

2.4 The implicit-explicit time discretization

The semi-discrete LDG schemes can be rewritten into the first-order ODE system

$$\frac{\mathrm{d}u}{\mathrm{d}t} = \mathcal{L}(t,u) + \mathcal{N}(t,u),$$

where $\mathcal{L}(t,u)$ arises from the spatial discretization of T_2 and will be treated implicitly, and $\mathcal{N}(t,u)$ is derived from the spatial discretization of T_1 and will be dealt with an explicit way. A third order IMEX Runge-Kutta (IMEX-RK) method will be considered in this paper. Given the numerical solution at time t^n, the IMEX-RK method forms 5 intermediate values $u^{n,s}$, $1 \le s \le 5$ according to

$$u^{n,s} = u^n + \tau \sum_{l=1}^{s} a_{sl} \mathcal{L}(t_l^n, u^{n,l}) + \tau \sum_{l=1}^{s-1} \hat{a}_{sl} \mathcal{N}(t_l^n, u^{n,l}), \tag{2.15a}$$

from which the approximation at time level t^{n+1} is assembled by

$$u^{n+1} = u^n + \tau \sum_{l=1}^{5} b_l \mathcal{L}(t_l^n, u^{n,l}) + \tau \sum_{l=1}^{5} \hat{b}_l \mathcal{N}(t_l^n, u^{n,l}), \tag{2.15b}$$

where the intermediate values $u^{n,s}$ are approximations to $u(x, t_l^n)$ and

$$t_l^n = t^n + \hat{c}_l \tau, \qquad \hat{c}_s = \sum_{l=1}^{s} a_{sl} = \sum_{l=1}^{s} \hat{a}_{sl}.$$

The IMEX-RK method can be represented by the following Butcher tableau

$$\begin{array}{|c|ccccc|ccccc|c|}
\hline
 & 0 & 0 & 0 & 0 & 0 & 0 & 0 & 0 & 0 & 0 & \\
 & 0 & \frac{1}{2} & 0 & 0 & 0 & \frac{1}{2} & 0 & 0 & 0 & 0 & \\
a_{sl} & 0 & \frac{1}{6} & \frac{1}{2} & 0 & 0 & \frac{11}{18} & \frac{1}{18} & 0 & 0 & 0 & \hat{a}_{sl} \\
 & 0 & -\frac{1}{2} & \frac{1}{2} & \frac{1}{2} & 0 & \frac{5}{6} & -\frac{5}{6} & \frac{1}{2} & 0 & 0 & \\
 & 0 & \frac{3}{2} & -\frac{3}{2} & \frac{1}{2} & \frac{1}{2} & \frac{1}{4} & \frac{7}{4} & \frac{3}{4} & -\frac{7}{4} & 0 & \\
\hline
b_l & 0 & \frac{3}{2} & -\frac{3}{2} & \frac{1}{2} & \frac{1}{2} & \frac{1}{4} & \frac{7}{4} & \frac{3}{4} & -\frac{7}{4} & 0 & \hat{b}_l \\
\hline
\end{array} \tag{2.16}$$

of which the left half lists a_{sl} and b_l, with the five rows from top to bottom corresponding to $s = 1, ..., 5$, and the columns from left to right corresponding to $l = 1, ..., 5$. Similarly, the right half lists $\hat{a}_{sl}$ and $\hat{b}_l$. With the above Butcher coefficients, we then arrive at a third order

IMEX-RK method. The IMEX-RK method we consider is a combination of a four-stage, third order, L-stable, stiffly-accurate, singly diagonally implicit Runge-Kutta method and a four-stage, third order explicit Runge-Kutta method. For more details of the method, we refer to [1]. We have also considered other IMEX methods, but we will not state them here to save space.

2.5 The choice of $a_1(x)$ for stability

Note that for the following simplified linear equations with periodic boundary conditions:

- The linear second order diffusion equation

$$U_t = dU_{xx},$$

- The linear dispersion equation

$$U_t + dU_{xxx} = 0,$$

- The linear fourth order diffusion equation

$$U_t + dU_{xxxx} = 0,$$

where $d > 0$ are three constants, the EIN-LDG schemes are shown to be unconditionally stable [14] provided $a_0 \geq 0.54$ regardless of the order accuracy of the LDG spatial discretizations. Here, we use the notation EIN-LDG to refer to both the VC-EIN-LDG and the CC-EIN-LDG schemes. After all, for linear equations with constant coefficients, these two schemes are equivalent. Even though the analysis is only performed on the simplified linear equations with constant coefficients, numerical experiments [14] show that the CC-EIN-LDG scheme is unconditionally stable for the second order diffusion equation (1.4) if

$$b_1 = a_0 \cdot \max d(u^n), \qquad a_0 \geq 0.54,$$

for the dispersion equation (2.10) if

$$b_1 = a_0 \cdot \max g'(u_x^n), \qquad a_0 \geq 0.54,$$

and for the fourth order diffusion equation (2.14) if

$$b_1 = a_0 \cdot \max d(u_x^n), \qquad a_0 \geq 0.54.$$

Based on the stability results of the CC-EIN-LDG schemes, we propose a guidance for the choice of $a_1(x)$ in the VC-EIN-LDG scheme for the second order diffusion equation (1.5), i.e.,

$$a_1(x) = a_0 \cdot \max_{t^n \leq t \leq t^{n+1}} d(u(x,t)), \qquad a_0 \geq 0.54, \tag{2.17}$$

for the dispersion equation (2.7), i.e.,

$$a_1(x) = a_0 \cdot \max_{t^n \leq t \leq t^{n+1}} g'(u_x(x,t)), \qquad a_0 \geq 0.54, \tag{2.18}$$

and for the fourth order diffusion equation (2.11), i.e.,

$$a_1(x) = a_0 \cdot \max_{t^n \leq t \leq t^{n+1}} d(u_x(x,t)), \qquad a_0 \geq 0.54. \tag{2.19}$$

Although the above stability conditions have not been confirmed theoretically, we find numerically that the above choices are sharp.

Note that for the quasi-linear equations, it is easy to obtain $a_1(x)$. However, if the diffusion coefficient or the dispersion coefficient depends on the solution (nonlinear case), as an alternative, the approach adopted in this paper is to obtain its approximation $\tilde{a}_1(x)$ through the convolution technique. Given a unit-mass kernel

$$\Phi(x) = \frac{1}{\int_{-1}^{1} e^{\frac{1}{|x|^2-1}} \mathrm{d}x} \begin{cases} e^{\frac{1}{|x|^2-1}}, & |x| < 1, \\ 0, & |x| \geq 1, \end{cases}$$

we form a dilated mollifier

$$\Phi_{C_0,\delta}(x) := \frac{C_0}{\delta} \Phi\left(\frac{x}{\delta}\right) \tag{2.20}$$

with C_0, δ being two free dilation parameters at our disposal. By tuning δ we can adjust the support of $\Phi(x)$ over the symmetric interval $(-\delta, \delta)$. By adjusting C_0, we can always make

$$\tilde{a}_1(x) = a_0 \cdot \tilde{d}(x) \geq a_1(x) = a_0 \cdot \max_{t^n \leq t \leq t^{n+1}} d(u(x,t)), \tag{2.21}$$

to keep the unconditional stability of the VC-EIN-LDG scheme for the second order diffusion equation, or

$$\tilde{a}_1(x) = a_0 \cdot \tilde{g}(x) \ \geq \ a_1(x) = a_0 \cdot \max_{t^n \leq t \leq t^{n+1}} g'(u_x(x,t)), \tag{2.22}$$

to keep the unconditional stability of the scheme for the dispersion equation, or

$$\tilde{a}_1(x) = a_0 \cdot \hat{d}(x) \ \geq \ a_1(x) = a_0 \cdot \max_{t^n \leq t \leq t^{n+1}} d(u_x(x,t)), \tag{2.23}$$

to keep the unconditional stability of the scheme for the fourth order diffusion equation, where

$$\begin{aligned}
\tilde{d}(x) &= \int d(u(y,t^n))\Phi_{C_0,\delta}(x-y)\,\mathrm{d}y, \\
\tilde{g}(x) &= \int g'(u_y(y,t^n))\Phi_{C_0,\delta}(x-y)\,\mathrm{d}y, \\
\hat{d}(x) &= \int d(u_y(y,t^n))\Phi_{C_0,\delta}(x-y)\,\mathrm{d}y.
\end{aligned}$$

However, now we encounter the difficulty on how to adjust the dilation parameters C_0 and δ. In the following, we provide a simple adjustment strategy using the second order diffusion equation as an example. At the beginning of the computation, we can always preset the parameters C_0 and δ according to $d(u^0)$. As the computation proceeds, we scan the sign of $\tilde{d}(x) - d(u^{n,s})$, where $u^{n,s}$, $2 \leq s \leq 5$ are the intermediate values defined by (2.15a), at some preselected points which are distributed inside each cell, for example, the Gaussian points used in the Gaussian numerical integration. For all the intermediate values $u^{n,s}$ between t^n and t^{n+1} time layers, if no negativity is detected at these points, then it is acceptable to judge that $\tilde{d}(x) - \max_{t^n \leq t \leq t^{n+1}} d(u(x,t))$ is nonnegative, and we make the parameters C_0 and δ stay the same as before. If $\tilde{d}(x) - d(u^{n,s})$ is negative at some points, then we return to the n-th time level and modify the parameters C_0 and δ according to $d(u^n)$. When the time step is relatively small, we can always obtain satisfactory parameters through a finite number of adjustments to ensure the stability of the scheme, provided the changes from $d(u^n)$ to $d(u^{n+1})$ are not particularly significant. It must be acknowledged that the adjustment strategy is still somewhat ad hoc, and it is worthwhile to make it more systematic and precise in future study.

Remark 2.1. *As pointed out in [14], the threshold value of* a_0 *for stability depends on the specific IMEX method, that is, the constant* $a_0 = 0.54$ *may not be valid if the IMEX time-marching method is changed.*

Remark 2.2. *The computational cost of the VC-EIN-LDG scheme is definitely higher than that of the CC-EIN-LDG scheme, especially in the high-dimensional nonlinear cases, as it requires performing convolution for a series of discrete points to get* $\tilde{a}_1(x)$*, reassembling the matrix and solving a more complex linear system at each time step. In addition, just as mentioned in the introduction, only in certain cases can the VC-EIN method obtain more accurate results than the CC-EIN method. First, it requires that the dominant error is due to the time-stepping or the spatial order of accuracy is at least the same as that of the time-marching method. Second, it requires that the diffusion coefficient or the dispersion coefficient has a few high and narrow bumps and the bumps only account for a small part of the whole computational domain. Therefore, we do not advocate blindly adopting the VC-EIN method, and would recommend using the CC-EIN method when it is not clear whether the diffusion coefficient or the dispersion coefficient meets the above requirements.*

3 The numerical experiments

In this section, we will present a series of numerical tests to show the order of accuracy and stability of the VC-EIN-LDG schemes for the high order diffusion and dispersion equations, respectively. We will also carry out a comparative study about the numerical performance of the VC-EIN-LDG and CC-EIN-LDG schemes. For simplicity, we only consider the one-dimensional and two-dimensional cases. Since the time discretization is limited to only third order accuracy, we concentrate on the piecewise quadratic polynomial ($k = 2$) case for the LDG spatial discretization in the numerical experiments. In addition, we take $\tau = h$ in the tests, such that the orders accuracy of errors in space and time match.

3.1 The second order diffusion equations

In this subsection, we would like to test the performance and stability of the proposed schemes for the second order diffusion equations in one and two space dimensions. The equations with periodic boundary conditions will be considered, unless otherwise stated. Following the lines in [6], it is straightforward to generalize the LDG scheme (2.2) for Cartesian meshes in the two-dimensional case.

3.1.1 The quasi-linear numerical test in one dimension

We consider the quasi-linear diffusion equation

$$U_t + \underbrace{(a_1(x)U_x)_x - (d(x,t)U_x)_x - s(x,t)}_{T_1} - \underbrace{(a_1(x)U_x)_x}_{T_2} = 0, \qquad x \in \left(-\frac{3}{2}\pi, \frac{1}{2}\pi\right) \tag{3.1}$$

augmented with the diffusion coefficient

$$d(x,t) = \alpha + \beta \tanh(\sigma \cos(\eta(x+t)))$$

the initial condition $U(x,0) = \sin(x)$ and the source term

$$\begin{aligned} s(x,t) = &\cos(x+t) + \beta\eta\sigma\cos(x+t)\,\mathrm{sech}^2(\sigma\cos(\eta(x+t)))\sin(\eta(x+t)) + \\ &\sin(x+t)(\alpha + \beta\tanh(\sigma\cos(\eta(x+t)))). \end{aligned}$$

The problem has an exact solution

$$U(x,t) = \sin(x+t). \tag{3.2}$$

Indeed, the standard IMEX methods can be directly adopted to solve the problem. To illustrate the necessity of the stability condition (2.17), in the test, we take $a_1(x)$ as $0.54 \cdot d(x,t^n)$, $0.53 \cdot \max_{t^n \le t \le t^{n+1}} d(x,t)$, $0.54 \cdot \max_{t^n \le t \le t^{n+1}} d(x,t)$ and $\max_{t^n \le t \le t^{n+1}} d(x,t)$, respectively. It is worth pointing out that it is not necessary to get the specific expression of $\max_{t^n \le t \le t^{n+1}} d(x,t)$. In the LDG scheme (2.2), these two formulas, (2.2b) and (2.2c), involve

$a_1(x) = a_0 \cdot \max_{t^n \le t \le t^{n+1}} d(x,t)$ and are integral expressions, which will be solved by a high order numerical integration method in practical computing. Thus we only need to consider the maximum value of $d(x,t)$ at a series of discrete time points from t^n to t^{n+1} for each numerical integration point and this is easy to achieve. We compute to $T = \pi$ with the parameters $\alpha = 11$, $\beta = 10$, $\sigma = 3\pi$, $\eta = 1$. Note that with those parameters, the diffusion coefficient $d(x,t)$ is not a monotonic function of time t for any fixed x. In other words, $d(x,t^n) \neq \max_{t^n \le t \le t^{n+1}} d(x,t)$. The numerical errors and orders of accuracy are listed in Table 3.1. Intuitively speaking, since u^{n+1} involves multiple intermediate values $u^{n,s}, 2 \le s \le 5$, as shown in (2.15), $a_1(x) < 0.54 \cdot \max_{t^n \le t \le t^{n+1}} d(x,t)$ is not large enough to remove the stiffness in all $\mathcal{N}(t^n_s, u^{n,s}), 2 \le s \le 5$ when $d(x,t)$ changes sharply with respect to time t and the mesh division is coarse, unless we use a small enough time step to temporally resolve the rapid transient of $d(x,t)$. Thus, from Table 3.1 we can see that the VC-EIN-LDG scheme is unstable or a sufficiently dense mesh grid is required to maintain the stability of the scheme if $a_1(x) < 0.54 \cdot \max_{t^n \le t \le t^{n+1}} d(x,t)$. When $a_1(x) \ge 0.54 \cdot \max_{t^n \le t \le t^{n+1}} d(x,t)$, the scheme is stable and the numerical orders of the scheme settle down towards the asymptotic value slowly. In fact, it is reasonable for this to happen, because the auxiliary term $(a_1(x)U_x)_x$ we add to and subtract from the equation are treated in different ways, i.e., one is treated explicitly and the other is treated implicitly. The two different time-stepping methods bring a certain error to the scheme, which increases with the increase of $a_1(x)$ and slows down the convergence of the scheme to the optimal order to some extent. The above explanation can also be used to interpret the similar convergence behavior of the VC-EIN-LDG and CC-EIN-LDG schemes for nonlinear equations.

Next, to demonstrate the optimal order of accuracy of the scheme, we consider again the quasi-linear numerical test proposed before. The simulation is run from $t = 0$ to $T = \pi$ with $a_1(x) = 0.54 \cdot \max_{t^n \le t \le t^{n+1}} d(x,t)$ and the parameters $\alpha = 1$, $\beta = \frac{1}{2}$, $\sigma = 1$, $\eta = 1$. We list the errors and the experimental orders of the VC-EIN-LDG scheme in Table 3.2, from which we can observe a rate of convergence about 3 for L^1, L^∞ and L^2 norms.

Table 3.1: The errors and orders of the VC-EIN-LDG scheme for Example (3.1) with $\alpha = 11$, $\beta = 10$, $\sigma = 3\pi$, $\eta = 1$.

$a_1(x)$	N	L^1 error	order	L^∞ error	order	L^2 error	order
$0.54 \cdot d(x, t^n)$	128	4.02E+21		9.84E+22		1.49E+22	
	256	2.02E+19	7.64	9.08E+20	6.76	1.00E+20	7.22
	512	2.24E+07	39.71	1.10E+09	39.59	1.21E+08	39.60
	1024	4.19E-06	42.28	2.83E-05	45.14	7.50E-06	43.87
	2048	8.68E-07	2.27	7.29E-06	1.96	1.73E-06	2.11
$0.53 \cdot \max\limits_{t^n \le t \le t^{n+1}} d(x,t)$	128	1.17E-03		1.91E-02		2.66E-03	
	256	6.87E-03	-2.55	2.83E-01	-3.89	3.21E-02	-3.59
	512	1.09E+03	-17.27	8.35E+04	-18.17	7.20E+03	-17.78
	1024	1.69E+16	-43.82	1.43E+18	-43.96	9.48E+16	-43.58
	2048	4.36E+46	-101.03	2.70E+48	-100.58	2.02E+47	-100.75
$0.54 \cdot \max\limits_{t^n \le t \le t^{n+1}} d(x,t)$	128	4.62E-04		2.23E-03		6.24E-04	
	256	1.04E-04	2.16	5.84E-04	1.93	1.49E-04	2.06
	512	2.12E-05	2.29	1.38E-04	2.08	3.39E-05	2.14
	1024	4.32E-06	2.29	3.27E-05	2.07	7.76E-06	2.13
	2048	8.78E-07	2.30	7.78E-06	2.07	1.76E-06	2.14
$\max\limits_{t^n \le t \le t^{n+1}} d(x,t)$	128	6.42E-04		2.27E-03		9.06E-04	
	256	1.55E-04	2.05	6.96E-04	1.71	2.28E-04	1.99
	512	3.43E-05	2.17	1.96E-04	1.83	5.46E-05	2.06
	1024	7.28E-06	2.24	5.22E-05	1.91	1.28E-05	2.09
	2048	1.48E-06	2.30	1.30E-05	2.01	2.92E-06	2.14

Table 3.2: The errors and orders of the VC-EIN-LDG scheme for Example (3.1) with $\alpha = 1$, $\beta = \frac{1}{2}$, $\sigma = 1$, $\eta = 1$.

$a_1(x)$	N	L^1 error	order	L^∞ error	order	L^2 error	order
$0.54 \cdot \max\limits_{t^n \le t \le t^{n+1}} d(x,t)$	128	2.33E-06		5.60E-06		2.94E-06	
	256	3.09E-07	2.91	7.72E-07	2.86	3.92E-07	2.91
	512	4.00E-08	2.95	1.02E-07	2.92	5.09E-08	2.95
	1024	5.09E-09	2.97	1.32E-08	2.95	6.50E-09	2.97
	2048	6.42E-10	2.99	1.68E-09	2.97	8.21E-10	2.98

3.1.2 The nonlinear numerical test in one dimension

We consider the nonlinear diffusion equation

$$U_t = (d(U)U_x)_x + s(x,t) \tag{3.3}$$

augmented with the diffusion coefficient

$$d(U) = \alpha + \beta U^2 \tag{3.4}$$

and the exact solution

$$U(x,t) = (\gamma + \lambda e^{-\sigma^2(1-\cos(x+t))})(\cos(\eta(x+t)) + 1).$$

The initial solution is extracted from the exact solution and the source term $s(x,t)$ is chosen properly such that the exact solution satisfies the given equation.

For such a nonlinear problem, since the stability condition (2.17) involves the unknown solutions above the n-th time level, the VC-EIN-LDG scheme is adjusted for use with the help of the convolution technique. In short, we add and subtract a second derivative term with variable coefficient $(\tilde{a}_1(x)U_x)_x$ at the left-hand side of the equation (3.3)

$$U_t + \underbrace{(\tilde{a}_1(x)U_x)_x - (d(U)U_x)_x - s(x,t)}_{T_1} - \underbrace{(\tilde{a}_1(x)U_x)_x}_{T_2} = 0,$$

where $\tilde{a}_1(x) = a_0 \cdot \tilde{d}(x)$ and $\tilde{d}(x)$ is the convolution of $d(u^n)$ and the dilated mollifier $\Phi_{C_0,\delta}(x)$ defined by (2.20). By adjusting the dilation parameters δ and C_0, we can always make $\tilde{a}_1(x)$ satisfy (2.21) and then ensure the stability of the scheme.

With the numerical solution at time t^n in hand, one might be tempted to increase the value of a_0 to make the inequality

$$a_0 \cdot d(u(x,t^n)) \geq 0.54 \cdot \max_{t^n \leq t \leq t^{n+1}} d(u(x,t))$$

tenable and ensure the stability of the scheme. However, this approach has two shortcomings that cannot be ignored. One is that much larger a_0 might be needed, which could bring larger errors. The other is that for degenerate parabolic equations, of which the diffusion coefficient $d(U)$ has a compact support, even if we increase the value of a_0, it still leads to $a_0 \cdot d(U) = 0$ outside the support. When the interface of the support is sharp and propagates with a high speed, it may still fail to remove the stiffness in all $\mathcal{N}(t_s^n, u^{n,s}), 2 \leq s \leq 5$ defined by (2.15), and ensure the stability of the scheme on a relatively coarse mesh grid. With the convolution of $d(u^n)$ and the dilated mollifier $\Phi_{C_0,\delta}(x)$, we can expand the support to avoid such a situation.

First, we numerically validate the stability of the VC-EIN-LDG scheme for this nonlinear problem. In the test, we take the parameters $\alpha = 0$, $\beta = 1$, $\gamma = 0$, $\lambda = 0.5$, $\sigma = 6$, $\eta = 4$. The computational domain is set to be $(-\pi, \pi)$ and the final computing time is $T = 1$. With these parameters, the diffusion coefficient $d(U)$, for any time $t \geq 0$, forms a steep bump with the value of $d(U)$ outside the bump decaying exponentially. To understand this clearly, we have plotted in Figure 3.1 the pictures for the diffusion coefficient $d(U(x,t))$ at time $t = 0$ and $t = 1$, respectively. The numerical results of the VC-EIN-LDG scheme with $\tilde{a}_1(x) = 0.54 \cdot \tilde{d}(x)$, $\tilde{a}_1(x) = \tilde{d}(x)$ $a_1(x) = 10 \cdot d(u^n)$ and $a_1(x) = 100 \cdot d(u^n)$ are presented in Table 3.3. Note that we preset the dilation parameters as $C_0 = 3$ and $\delta = 0.6$ in the test. These two preset values are sufficient to ensure the stability of the scheme without adjustment, due to the fact that the bump of the diffusion coefficient does not deform except for moving. As expected, the scheme is stable for $\tilde{a}_1(x) \geq 0.54 \cdot \max_{t^n \leq t \leq t^{n+1}} d(u(x,t))$. In addition, even though we greatly increase the value of a_0 in the test, $a_1(x) = a_0 \cdot d(u^n)$ still cannot ensure the stability of the scheme, unless the mesh is dense enough. When $N = 2048$, the VC-EIN-LDG scheme is stable for $a_1(x) = 10 \cdot d(u^n)$, however, the errors of the scheme are much larger than those of the scheme with $\tilde{a}_1(x) = 0.54 \cdot \tilde{d}(x)$.

Second, we perform an optimal accuracy check for the VC-EIN-LDG and CC-EIN-LDG schemes. In the test, we take the parameters $\alpha = 0$, $\beta = 2$, $\gamma = 0.01$, $\lambda = 0.1$, $\sigma = 3$, $\eta = 4$. Compared with the previous case, we reduce the values of these two parameters, λ and σ, and increase the values of β and γ. With these parameters, the diffusion coefficient $d(U)$, for any time $t \geq 0$, forms a gentler bump and the value of $d(U)$ outside the bump no longer decays exponentially. To understand this clearly, we have plotted in Figure 3.2 the pictures for the diffusion coefficient $d(U(x,t))$ at time $t = 0$ and $t = 1$, respectively. On the basis of keeping the final computing time and the computational domain unchanged, the simulation is run with $\tilde{a}_1(x) = 0.54 \cdot \tilde{d}(x)$ and $b_1 = 0.54 \cdot \max d(u^n)$. Note that for the VC-EIN-LDG scheme, the dilation parameters are kept as $C_0 = 2.2$, $\delta = 0.7$ and remain unchanged in this test. The orders and errors of the schemes in the L^1, L^2 and L^∞ norms are presented in Table 3.4. Clearly, we can observe a rate of convergence about 3 for all the norms. In addition, in this case, the errors of the VC-EIN-LDG scheme are slightly smaller compared to those of the CC-EIN-LDG scheme.

Third, we increase the deviation of the bump and compare the performance of both the schemes. On the basis of keeping other parameters of the previous case unchanged, the value of λ is increased to 1. Note that for the VC-EIN-LDG scheme, we still set the dilation parameters as $C_0 = 2.2$ and $\delta = 0.7$ in the test. The errors and orders of accuracy for both the schemes are computed at two different regions, namely the entire computational region $[-\pi, \pi]$ and the region away from the bumps $[-\pi, -2] \cup [1, \pi]$. The results are listed in Table 3.5 and Table 3.6, respectively. Due to the fact the errors are larger near the bumps and such errors do not decrease much from the CC-EIN method to the VC-EIN method, all the global errors (L^1, L^2, L^∞) do not show significant reductions from the CC-EIN-LDG scheme to the VC-EIN-LDG scheme as can be seen in Table 3.5. However, in regions away from the bumps, the VC-EIN method produces much smaller errors than the CC-EIN method, as can be seen in Table 3.6.

3.1.3 The nonlinear numerical test in one dimension

We experiment with a highly nonlinear example

$$U_t = (d(U)U_x)_x + s(x,t), \tag{3.5a}$$

$$d(U) = (\gamma + \lambda e^{-\sigma^2(1-U)})(2U^2 - 1)^2 \tag{3.5b}$$

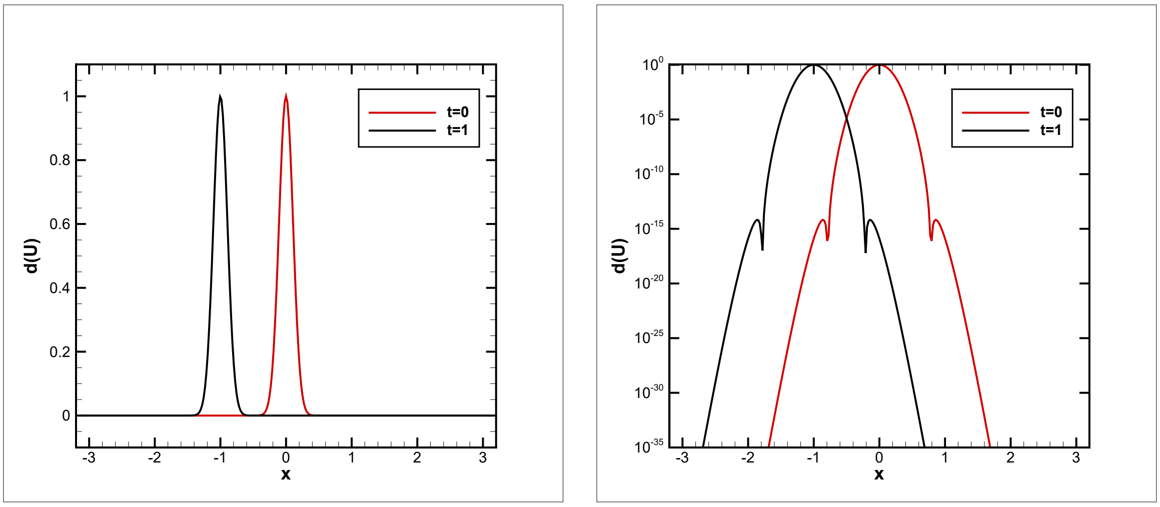

Figure 3.1: *Snapshots of the diffusion coefficient* (3.4) *with parameters* $\alpha = 0$, $\beta = 1$, $\gamma = 0$, $\lambda = 0.5$, $\sigma = 6$, $\eta = 4$ *at the indicated times.*

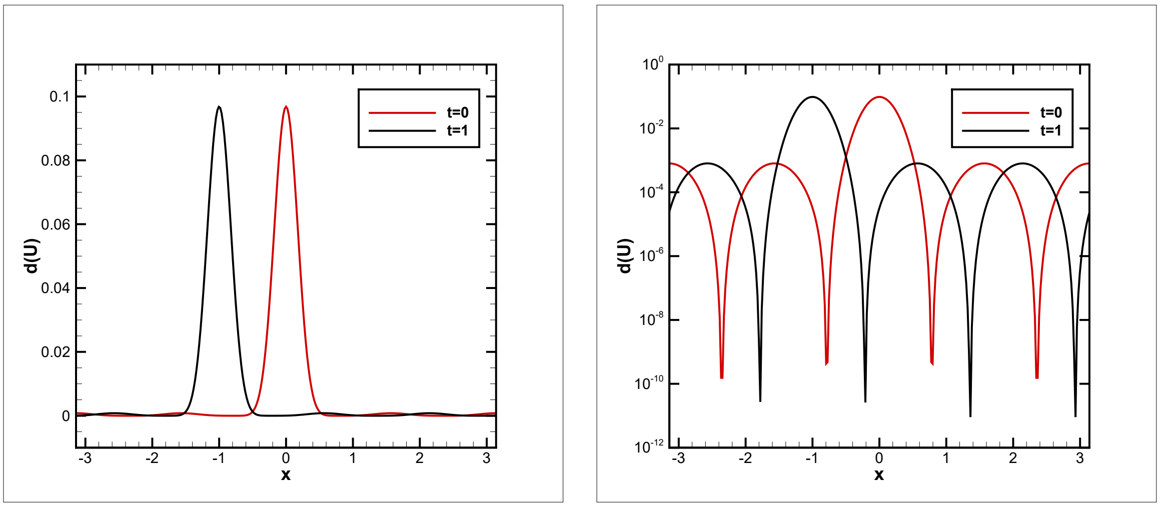

Figure 3.2: *Snapshots of the diffusion coefficient* (3.4) *with parameters* $\alpha = 0$, $\beta = 2$, $\gamma = 0.01$, $\lambda = 0.1$, $\sigma = 3$, $\eta = 4$ *at the indicated times.*

Table 3.3: The errors and orders of the VC-EIN-LDG scheme for Example (3.3) with $\alpha = 0$, $\beta = 1$, $\gamma = 0$, $\lambda = 0.5$, $\sigma = 6$, $\eta = 4$.

	N	L^1 error	order	L^∞ error	order	L^2 error	order
$\tilde{a}_1(x) = 0.54 \cdot \tilde{d}(x)$	128	2.29E-03		4.19E-02		6.05E-03	
	256	6.60E-04	1.80	9.72E-03	2.11	1.65E-03	1.87
	512	1.68E-04	1.97	1.89E-03	2.36	4.19E-04	1.98
	1024	3.68E-05	2.19	5.53E-04	1.77	9.40E-05	2.16
	2048	6.82E-06	2.43	1.21E-04	2.20	1.80E-05	2.38
$\tilde{a}_1(x) = \tilde{d}(x)$	128	4.72E-03		8.59E-02		1.23E-02	
	256	1.63E-03	1.54	2.61E-02	1.72	4.11E-03	1.58
	512	5.00E-04	1.70	6.38E-03	2.03	1.25E-03	1.71
	1024	1.33E-04	1.92	1.90E-03	1.74	3.41E-04	1.88
	2048	2.94E-05	2.17	5.32E-04	1.84	7.92E-05	2.11
$a_1(x) = 10 \cdot d(u^n)$	128	2.62E-01		8.89E+00		8.12E-01	
	256	NaN	NaN	NaN	NaN	NaN	NaN
	512	NaN	NaN	NaN	NaN	NaN	NaN
	1024	NaN	NaN	NaN	NaN	NaN	NaN
	2048	3.10E-03	NaN	7.13E-02	NaN	9.14E-03	NaN
$a_1(x) = 100 \cdot d(u^n)$	128	NaN		NaN		NaN	
	256	1.98E-01	NaN	1.62E+01	NaN	1.06E+00	NaN
	512	1.83E-01	0.12	2.84E+01	-0.81	1.33E+00	-0.32
	1024	NaN	NaN	NaN	NaN	NaN	NaN
	2048	NaN	NaN	NaN	NaN	NaN	NaN

Table 3.4: The errors and orders of the VC-EIN-LDG and CC-EIN-LDG schemes for Example (3.3) with $\alpha = 0$, $\beta = 2$, $\gamma = 0.01$, $\lambda = 0.1$, $\sigma = 3$, $\eta = 4$.

VC-EIN-LDG

$\tilde{a}_1(x)$	N	L^1 error	order	L^∞ error	order	L^2 error	order
$0.54 \cdot \tilde{d}(x)$	128	5.78E-06		7.14E-05		1.17E-05	
	256	7.30E-07	2.99	9.12E-06	2.97	1.49E-06	2.97
	512	9.36E-08	2.96	1.16E-06	2.98	1.92E-07	2.96
	1024	1.19E-08	2.97	1.46E-07	2.99	2.46E-08	2.97
	2048	1.51E-09	2.98	1.83E-08	2.99	3.11E-09	2.98

CC-EIN-LDG

b_1	N	L^1 error	order	L^∞ error	order	L^2 error	order
$0.54 \cdot \max d(u^n)$	128	7.67E-06		7.57E-05		1.40E-05	
	256	9.96E-07	2.94	9.49E-06	3.00	1.83E-06	2.93
	512	1.30E-07	2.94	1.22E-06	2.97	2.40E-07	2.93
	1024	1.66E-08	2.96	1.53E-07	2.99	3.10E-08	2.96
	2048	2.11E-09	2.98	1.92E-08	2.99	3.93E-09	2.98

Table 3.5: The errors and orders of the VC-EIN-LDG and CC-EIN-LDG schemes for Example (3.3) with $\alpha = 0$, $\beta = 2$, $\gamma = 0.01$, $\lambda = 1$, $\sigma = 3$, $\eta = 4$ in $[-\pi, \pi]$.

VC-EIN-LDG

$\tilde{a}_1(x)$	N	L^1 error	order	L^∞ error	order	L^2 error	order
$0.54 \cdot \tilde{d}(x)$	128	2.12E-02		2.88E-01		4.82E-02	
	256	6.15E-03	1.79	7.60E-02	1.92	1.32E-02	1.87
	512	1.52E-03	2.01	1.50E-02	2.34	3.03E-03	2.12
	1024	3.33E-04	2.19	2.37E-03	2.66	6.33E-04	2.26
	2048	7.29E-05	2.19	6.60E-04	1.85	1.51E-04	2.06

CC-EIN-LDG

b_1	N	L^1 error	order	L^∞ error	order	L^2 error	order
$0.54 \cdot \max d(u^n)$	128	2.62E-02		1.34E-01		3.84E-02	
	256	1.19E-02	1.14	5.23E-02	1.36	1.76E-02	1.13
	512	4.69E-03	1.34	3.03E-02	0.79	7.59E-03	1.21
	1024	1.58E-03	1.57	1.38E-02	1.13	2.84E-03	1.42
	2048	4.36E-04	1.86	4.72E-03	1.55	8.52E-04	1.74

Table 3.6: The errors and orders of the VC-EIN-LDG and CC-EIN-LDG schemes for Example (3.3) with $\alpha = 0$, $\beta = 2$, $\gamma = 0.01$, $\lambda = 1$, $\sigma = 3$, $\eta = 4$ in $[-\pi, -2] \cup [1, \pi]$.

VC-EIN-LDG

$\tilde{a}_1(x)$	N	L^1 error	order	L^∞ error	order	L^2 error	order
$0.54 \cdot \tilde{d}(x)$	128	1.95E-06		1.40E-04		1.24E-05	
	256	2.12E-07	3.20	2.17E-05	2.69	1.50E-06	3.05
	512	1.55E-08	3.78	1.70E-06	3.68	9.71E-08	3.95
	1024	1.14E-09	3.77	8.16E-08	4.38	4.33E-09	4.49
	2048	1.21E-10	3.24	5.88E-09	3.79	3.21E-10	3.75

CC-EIN-LDG

b_1	N	L^1 error	order	L^∞ error	order	L^2 error	order
$0.54 \cdot \max d(u^n)$	128	1.04E-02		2.98E-02		1.39E-02	
	256	4.06E-03	1.35	2.11E-02	0.50	6.46E-03	1.11
	512	9.07E-04	2.16	8.67E-03	1.28	1.85E-03	1.80
	1024	1.82E-04	2.32	1.69E-03	2.36	3.11E-04	2.57
	2048	5.05E-05	1.85	2.81E-04	2.59	9.47E-05	1.72

augmented with the exact solution

$$U(x,t) = \cos(x+t).$$

The initial solution is extracted from the exact solution and the source term $s(x,t)$ is chosen properly such that the exact solution satisfies the given equation.

First, we numerically validate the stability and error accuracy of the VC-EIN-LDG scheme. In the test, we take the parameters $\gamma = 0$, $\lambda = 20$, $\sigma = 3$. The computational domain is set to be $(-\pi, \pi)$ and the final computing time is $T = 1$. The numerical results of the scheme with $a_1(x) = 1000 \cdot d(u^n)$ and $\tilde{a}_1(x) = 0.54 \cdot \tilde{d}(x)$ are presented in Table 3.7. Note that for the VC-EIN-LDG scheme, the dilation parameters are set as $C_0 = 1.8$, $\delta = 0.7$ and remain unchanged in the test. As expected, the scheme is stable for $\tilde{a}_1(x) = 0.54 \cdot \tilde{d}(x)$. Even though we greatly increase the value of a_0 to 1000, $a_1(x) = a_0 \cdot d(u^n)$ still cannot ensure the stability of the scheme. Second, the CC-EIN-LDG scheme is also used to solve the nonlinear problem. In the test, we take $b_1 = 0.54 \cdot \max d(u^n)$. The numerical results of the scheme are also listed in Table 3.7, from which we can see that the CC-EIN-LDG scheme is stable as always and the numerical orders of accuracy settle down towards the asymptotic value slowly with mesh refinements. Due to the fact the errors are larger near the bumps and such errors do not decrease much from the CC-EIN method to the VC-EIN method, the global errors of the VC-EIN-LDG scheme are comparable with the CC-EIN-LDG scheme. However, in regions away from the bumps, namely $[-\pi, -2.5] \cup [1.5, \pi]$, the VC-EIN method produces much smaller errors than the CC-EIN method, as can be seen in Table 3.8.

Table 3.7: The errors and orders of the VC-EIN-LDG and CC-EIN-LDG schemes for Example (3.5) with $\gamma = 0$, $\lambda = 20$, $\sigma = 3$ in $[-\pi, \pi]$.

VC-EIN-LDG

	N	L^1 error	order	L^∞ error	order	L^2 error	order
$a_1(x) = 1000 \cdot d(u^n)$	128	NaN		NaN		NaN	
	256	4.08E-01	NaN	2.72E+00	NaN	7.18E-01	NaN
	512	NaN	NaN	NaN	NaN	NaN	NaN
	1024	NaN	NaN	NaN	NaN	NaN	NaN
	2048	NaN	NaN	NaN	NaN	NaN	NaN
$\tilde{a}_1(x) = 0.54 \cdot \tilde{d}(x)$	128	4.56E-03		6.70E-02		1.15E-02	
	256	1.18E-03	1.95	2.06E-02	1.70	3.11E-03	1.89
	512	2.56E-04	2.20	5.17E-03	2.00	7.08E-04	2.14
	1024	5.00E-05	2.36	1.07E-03	2.27	1.37E-04	2.37
	2048	8.14E-06	2.62	1.84E-04	2.54	2.25E-05	2.61

CC-EIN-LDG

	N	L^1 error	order	L^∞ error	order	L^2 error	order
$b_1 = 0.54 \cdot \max d(u^n)$	128	5.13E-03		1.17E-02		6.31E-03	
	256	9.22E-04	2.48	2.59E-03	2.18	1.14E-03	2.47
	512	1.44E-04	2.68	5.76E-04	2.17	1.81E-04	2.66
	1024	2.12E-05	2.76	1.31E-04	2.14	2.85E-05	2.66
	2048	2.96E-06	2.84	2.77E-05	2.24	4.72E-06	2.60

3.1.4 Numerical simulation to the porous medium equation

To further validate the performance of the proposed schemes, we consider the porous medium equation (PME)

$$U_t = (U^m)_{xx}, \tag{3.6}$$

Table 3.8: The errors and orders of the VC-EIN-LDG and CC-EIN-LDG schemes for Example (3.5) with $\gamma = 0$, $\lambda = 20$, $\sigma = 3$ in $[-\pi, -2.5] \cup [1.5, \pi]$.

VC-EIN-LDG							
$\tilde{a}_1(x)$	N	L^1 error	order	L^∞ error	order	L^2 error	order
$0.54 \cdot \tilde{d}(x)$	128	8.25E-07		3.52E-06		1.14E-06	
	256	9.42E-08	3.13	3.31E-07	3.41	1.21E-07	3.23
	512	1.01E-08	3.22	3.09E-08	3.42	1.24E-08	3.30
	1024	1.08E-09	3.23	2.82E-09	3.46	1.27E-09	3.28
	2048	1.18E-10	3.19	2.76E-10	3.35	1.34E-10	3.25
CC-EIN-LDG							
b_1	N	L^1 error	order	L^∞ error	order	L^2 error	order
$0.54 \cdot \max d(u^n)$	128	4.51E-03		8.81E-03		5.13E-03	
	256	7.66E-04	2.56	1.51E-03	2.54	8.72E-04	2.56
	512	1.12E-04	2.77	2.17E-04	2.81	1.27E-04	2.78
	1024	1.56E-05	2.84	2.90E-05	2.90	1.76E-05	2.85
	2048	2.09E-06	2.90	3.96E-06	2.87	2.36E-06	2.90

where $m \geq 1$ is a constant. This equation [21] often occurs in nonlinear problems of heat and mass transfer, combustion theory, and flow in porous media, where U is either a concentration or a temperature required to be nonnegative. We assume the initial value for the above equation is a bounded nonnegative continuous function. Then the PME can be rewritten as

$$U_t = (d(U)U_x)_x$$

with $d(U) = mU^{m-1}$. In this case, the classical smooth solution may not always exist in general, even if the initial solution is smooth. It is necessary to consider the weak energy solution. In a recent work [16], a second order CC-EIN method with the third order LDG spatial discretization for the PME with the Barenblatt solution was considered. We try to replicate this test with the third order VC-EIN-LDG and CC-EIN-LDG schemes in this paper. For any given $m \geq 1$, the Barenblatt solution is defined by

$$U(x,t) = t^{-s} \left[\left(1 - \frac{s(m-1)}{2m} \frac{|x|^2}{t^{2s}} \right)_+ \right]^{1/(m-1)}$$

where $u_+ = \max\{u, 0\}$ and $s = 1/(m+1)$. Similarly, we begin the computation from $t = 1$ in order to avoid the singularity of the Barenblatt solution near $t = 0$. The boundary condition is $U(\pm 6, t) = 0$ for $t > 1$. Note that the simulation is run with $\tilde{a}_1(x) = 0.54 \cdot \tilde{d}(x)$ and $b_1 = 0.54 \cdot \max d(u^n)$. In addition, the dilation parameters are always taken as $C_0 = 1.2$, $\delta = 2.5$ for the VC-EIN-LDG scheme. We plot in Figure 3.3 the numerical results for $m = 3$ and $m = 8$ at $T = 2$ with $N = 800$. From this figure, we see that our schemes simulate the Barenblatt solution accurately and sharply.

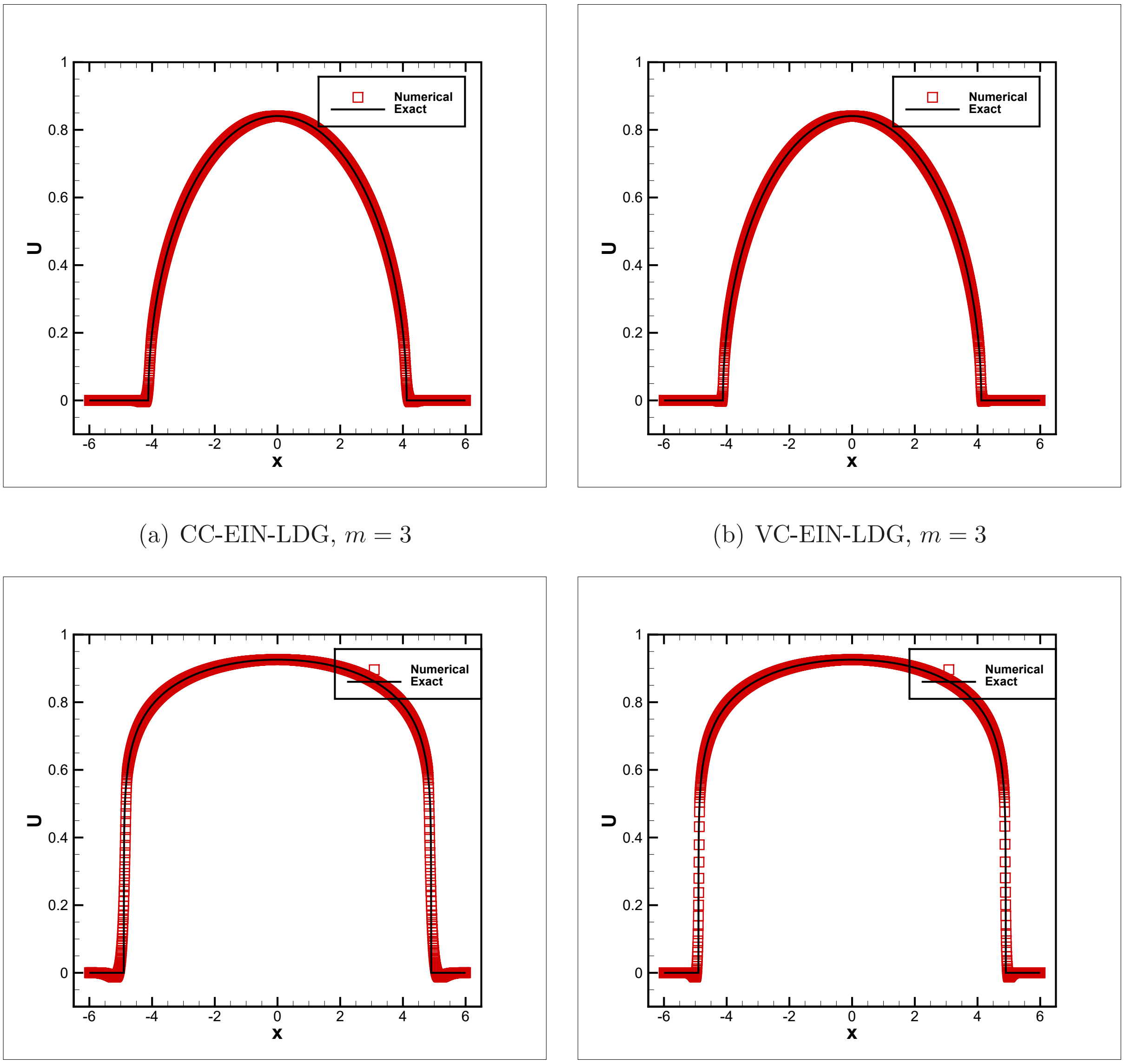

(a) CC-EIN-LDG, $m = 3$

(b) VC-EIN-LDG, $m = 3$

(c) CC-EIN-LDG, $m = 8$

(d) VC-EIN-LDG, $m = 8$

Figure 3.3: The CC-EIN-LDG and VC-EIN-LDG schemes for the PME (3.6) with the Barenblatt solution at $T = 2$. Solid line: the exact solution; Square symbol: the numerical solution.

3.1.5 The nonlinear numerical test in two dimensions

We consider the two-dimensional nonlinear diffusion equation

$$U_t = \nabla \cdot (d(U)\nabla U) + s(x, y, t) \tag{3.7}$$

augmented with the diffusion coefficient (3.4) and the exact solution

$$U(x, y, t) = (\gamma + \lambda e^{-\sigma^2(1-\cos(x+y+t))})(1 + \cos(\eta(x + y + t))).$$

The initial solution is extracted from the exact solution and the source term $s(x, y, t)$ is chosen properly such that the exact solution satisfies the given equation.

First, we numerically validate the stability and error accuracy of the VC-EIN-LDG scheme. In the test, we take the parameters $\alpha = 0$, $\beta = 2$, $\gamma = 0.001$, $\lambda = 0.1$, $\sigma = 3$, $\eta = 4$. The computational domain is set to be $(-\pi, \pi)^2$ and the final computing time is $T = 1$. The numerical results of the scheme with $a_1(x, y) = 0.54 \cdot d(u^n)$ and $\tilde{a}_1(x, y) = 0.54 \cdot \tilde{d}(x, y)$ are presented in Table 3.9. Note that for the VC-EIN-LDG scheme, the dilation parameters are set as $C_0 = 2$, $\delta = 0.6$ and remain unchanged in the test. It is observed that the scheme is stable for $\tilde{a}_1(x, y) = 0.54 \cdot \tilde{d}(x, y)$ and can achieve very nice third order convergence rates for L^1, L^2 and L^∞ norms. Second, the CC-EIN-LDG scheme is also used to solve the nonlinear problem. In the test, we take $b_1 = 0.54 \cdot \max d(u^n)$. The numerical results of the scheme are also listed in Table 3.9, from which we can see that the CC-EIN-LDG scheme is stable as always. Under the same mesh grid, the results of the VC-EIN-LDG scheme are compared against those of the CC-EIN-LDG scheme. In this case, the global errors of the VC-EIN-LDG scheme are comparable with the CC-EIN-LDG scheme.

3.2 The dispersion equations

In this subsection, we would like to test the performance and stability of the proposed schemes for the dispersion equations in one and two space dimensions. The equations with periodic boundary conditions will be considered, unless otherwise stated. The generalization

Table 3.9: The errors and orders of the VC-EIN-LDG and CC-EIN-LDG schemes for Example (3.7) with $\alpha = 0$, $\beta = 2$, $\gamma = 0.001$, $\lambda = 0.1$, $\sigma = 3$, $\eta = 4$.

VC-EIN-LDG							
	N	L^1 error	order	L^∞ error	order	L^2 error	order
$a_1(x, y) = 0.54 \cdot d(u^n)$	20	3.58E+04		1.58E+06		1.36E+05	
	40	NaN	NaN	NaN	NaN	NaN	NaN
	60	NaN	NaN	NaN	NaN	NaN	NaN
	80	NaN	NaN	NaN	NaN	NaN	NaN
	100	NaN	NaN	NaN	NaN	NaN	NaN
$\tilde{a}_1(x, y) = 0.54 \cdot \tilde{d}(x, y)$	20	5.97E-03		6.88E-02		1.34E-02	
	40	7.00E-04	3.09	1.55E-02	2.15	1.70E-03	2.97
	60	1.56E-04	3.70	3.47E-03	3.70	3.67E-04	3.79
	80	6.33E-05	3.13	9.26E-04	4.59	1.44E-04	3.25
	100	3.08E-05	3.23	4.37E-04	3.36	7.01E-05	3.22

CC-EIN-LDG							
	N	L^1 error	order	L^∞ error	order	L^2 error	order
$b_1 = 0.54 \cdot \max d(u^n)$	20	3.03E-03		3.15E-02		6.21E-03	
	40	6.04E-04	2.33	1.30E-02	1.27	1.37E-03	2.18
	60	1.34E-04	3.70	3.08E-03	3.55	3.10E-04	3.66
	80	5.67E-05	3.00	9.77E-04	4.00	1.24E-04	3.18
	100	2.99E-05	2.88	4.56E-04	3.41	6.34E-05	3.01

of the LDG scheme (2.8) to the two-dimensional dispersion equations is straightforward; we refer the readers to [19] for the details.

3.2.1 The quasi-linear numerical test in one dimension

Indeed, the standard IMEX methods can be directly adopted to solve the quasi-linear equations. In order to illustrate the necessity of the stability condition (2.18), we consider the quasi-linear dispersion equation

$$U_t + \underbrace{[(g(x,t) - a_1(x))U_x]_{xx} - s(x,t)}_{T_1} + \underbrace{(a_1(x)U_x)_{xx}}_{T_2} = 0, \qquad x \in (0, 2\pi) \tag{3.8}$$

augmented with the dispersion coefficient

$$g(x,t) = \alpha - \beta \tanh^2(\eta \cos(x+t)),$$

the initial condition $U(x,0) = \sin(x)$ and the source term

$$\begin{aligned} s(x,t) = &- 2\beta\eta^2 \cos(x+t) \operatorname{sech}^4(\eta\cos(x+t)) \sin^2(x+t) + \\ &2\beta\eta \operatorname{sech}^2(\eta\cos(x+t)) \tanh(\eta\cos(x+t))(\cos^2(x+t) - \\ &2\sin^2(x+t) + 2\eta\cos(x+t)\sin^2(x+t)\tanh(\eta\cos(x+t))) + \\ &\cos(x+t)(1 - \alpha + \beta\tanh^2(\eta\cos(x+t))). \end{aligned}$$

The exact solution to the problem is defined by (3.2). In order to test the stability of the VC-EIN-LDG scheme in terms of $a_1(x)$, in the test, we take $a_1(x)$ as $0.54 \cdot g(x, t^n)$, $0.53 \cdot \max_{t^n \le t \le t^{n+1}} g(x,t)$, $0.54 \cdot \max_{t^n \le t \le t^{n+1}} g(x,t)$ and $\max_{t^n \le t \le t^{n+1}} g(x,t)$, respectively. We compute to $T = 10$ with the parameters $\alpha = 1$, $\beta = 1$, $\eta = 3$. We present the errors and orders of accuracy in different norms in Table 3.10, from which we can see that the scheme is unstable or a sufficiently dense mesh grid is required to maintain the stability of the scheme if $a_1(x) < 0.54 \cdot \max_{t^n \le t \le t^{n+1}} g(x,t)$. As expected, when $a_1(x) = 0.54 \cdot \max_{t^n \le t \le t^{n+1}} g(x,t)$, the VC-EIN-LDG scheme is stable and can achieve a very nice third order convergence rate. The scheme remains stable as always when $a_1(x) = \max_{t^n \le t \le t^{n+1}} g(x,t)$, but the numerical orders of accuracy settle down towards the asymptotic value slowly.

Table 3.10: The errors and orders of the VC-EIN-LDG scheme for Example (3.8) with $\alpha = 1$, $\beta = 1$, $\eta = 3$.

$a_1(x)$	N	L^1 error	order	L^∞ error	order	L^2 error	order
$0.54 \cdot g(x, t^n)$	64	5.47E+50		5.00E+51		1.25E+51	
	128	1.06E+53	-7.60	1.18E+54	-7.88	2.65E+53	-7.72
	256	3.51E+46	21.52	4.63E+47	21.28	9.52E+46	21.41
	512	3.89E+25	69.61	5.72E+26	69.46	1.13E+26	69.51
	1024	6.30E-06	102.28	2.02E-05	104.48	7.93E-06	103.50
$0.53 \cdot \max\limits_{t^n \le t \le t^{n+1}} g(x,t)$	64	4.62E-02		1.15E-01		5.53E-02	
	128	5.34E-03	3.11	1.28E-02	3.17	6.32E-03	3.13
	256	4.90E-04	3.44	1.28E-03	3.32	5.76E-04	3.46
	512	5.54E+20	-79.90	7.51E+21	-82.27	1.46E+21	-81.07
	1024	4.01E+70	-165.63	5.73E+71	-165.71	1.08E+71	-165.66
$0.54 \cdot \max\limits_{t^n \le t \le t^{n+1}} g(x,t)$	64	4.64E-02		1.16E-01		5.55E-02	
	128	5.34E-03	3.12	1.28E-02	3.17	6.32E-03	3.13
	256	4.92E-04	3.44	1.16E-03	3.47	5.73E-04	3.46
	512	4.69E-05	3.39	1.09E-04	3.41	5.61E-05	3.35
	1024	5.86E-06	3.00	1.36E-05	3.00	7.06E-06	2.99
$\max\limits_{t^n \le t \le t^{n+1}} g(x,t)$	64	1.17E-02		3.10E-02		1.43E-02	
	128	2.97E-04	5.30	1.09E-03	4.83	4.00E-04	5.16
	256	9.24E-05	1.69	2.92E-04	1.90	1.18E-04	1.77
	512	2.21E-05	2.06	8.52E-05	1.78	2.86E-05	2.04
	1024	5.41E-06	2.03	2.09E-05	2.02	6.88E-06	2.06

3.2.2 The nonlinear numerical test in one dimension

We consider the nonlinear dispersion equation

$$U_t + g(U_x)_{xx} = s(x,t) \tag{3.9}$$

augmented with the dispersion coefficient

$$g(U_x) = \alpha U_x + \beta U_x^3$$

and the exact solution

$$U(x,t) = \gamma \sin(\eta(x+t)) - \lambda \tanh(\sigma \cos(x+t)).$$

The initial solution is extracted from the exact solution and the source term $s(x,t)$ is chosen properly such that the exact solution satisfies the given equation.

Similarly, for such a nonlinear problem, since the stability condition (2.18) involves the unknown solutions above the n-th time layer, the VC-EIN-LDG scheme is adjusted for use with the help of the convolution technique. In short, we add and subtract a third derivative term with variable coefficient $(\tilde{a}_1(x)U_x)_{xx}$ at the left-hand side of the equation

$$U_t + \underbrace{g(U_x)_{xx} - (\tilde{a}_1(x)U_x)_{xx} - s(x,t)}_{T_1} + \underbrace{(\tilde{a}_1(x)U_x)_{xx}}_{T_2} = 0,$$

where $\tilde{a}_1(x) = a_0 \cdot \tilde{g}(x)$ and $\tilde{g}(x)$ is the convolution of $g'(u_x^n)$ and the dilated mollifier $\Phi_{C_0,\delta}(x)$ defined by (2.20). By adjusting the dilation parameters δ and C_0, we can always make inequality (2.22) tenable to ensure the stability of the VC-EIN-LDG scheme. The adjustment strategy of the dilation parameters δ and C_0 is similar to that described in Section 2.3 for the second order diffusion equations.

First, we test the stability of the VC-EIN-LDG scheme for this nonlinear dispersion equation. In the test, we take the parameters $\alpha = 0.001$, $\beta = 0.1$, $\gamma = -0.2$, $\lambda = 0.2$, $\sigma = 2$, $\eta = 2$. The computational domain is set to be $(-\pi, \pi)$ and the final computing time is $T = 1$. The numerical results of the VC-EIN-LDG scheme with $a_1(x) = 0.54 \cdot g'(u_x^n)$,

$a_1(x) = g'(u_x^n)$, $\tilde{a}_1(x) = 0.54 \cdot \tilde{g}(x)$ and $\tilde{a}_1(x) = \tilde{g}(x)$ are presented in Table 3.11. Note that the dilation parameters are set as $C_0 = 1.5$, $\delta = 0.5$ and remain unchanged in the test. As expected, the scheme is stable and can achieve optimal error accuracy if $\tilde{a}_1(x) \geq 0.54 \cdot \tilde{g}(x)$.

Second, we take the parameters $\alpha = 0.001$, $\beta = 0.025$, $\gamma = -0.05$, $\lambda = 0.05$, $\sigma = 4$, $\eta = 2$ to demonstrate the optimal accuracy of the VC-EIN-LDG and CC-EIN-LDG schemes in various norms. On the basis of keeping the final computing time and the computational domain unchanged, the simulation is run with $\tilde{a}_1(x) = 0.54 \cdot \tilde{g}(x)$ and $b_1 = 0.54 \cdot \max g'(u_x^n)$. Note that in the test we keep the dilation parameters $C_0 = 2$, $\delta = 0.7$ unchanged for the VC-EIN-LDG scheme. The numerical errors and orders of accuracy are presented in Table 3.12, from which we can see that both the schemes are stable as always and can achieve optimal orders of accuracy for all the norms. In addition, compared with the CC-EIN-LDG scheme, the VC-EIN-LDG scheme is more accurate for this test.

Third, we take $\alpha = 0.001$, $\beta = 0.1$, $\gamma = -0.1$, $\lambda = 0.1$, $\sigma = 4$, $\eta = 2$ and compare the performance of the VC-EIN-LDG scheme with the CC-EIN-LDG scheme. Compared with the previous case, we have reduced the value of γ and increased the values of β and λ. With these parameters, there is a larger deviation in $g'(U_x)$ and the bump of $g'(U_x)$ tends to be steeper. To understand this clearly, we have plotted in Figure 3.4 the pictures for $g'(U_x)$ at time $t = 0$ and $t = 1$, respectively. Note that for the VC-EIN-LDG scheme, we set the dilation parameters as $C_0 = 3.3$ and $\delta = 0.7$ in the test. The errors and orders of accuracy of these two schemes are listed in Table 3.13. In this case, the errors of the VC-EIN-LDG scheme are smaller than those of the CC-EIN-LSG scheme.

3.2.3 The nonlinear numerical test in one dimension

We experiment with a highly nonlinear example

$$U_t + g(U_x)_{xx} = s(x,t), \qquad x \in (0, 2\pi) \tag{3.10a}$$

$$g(U_x) = \alpha U_x + \tanh(e^{\beta(1+U_x)}). \tag{3.10b}$$

Table 3.11: The errors and orders of the VC-EIN-LDG scheme for Example (3.9) with $\alpha = 0.001$, $\beta = 0.1$, $\gamma = -0.2$, $\lambda = 0.2$, $\sigma = 2$, $\eta = 2$.

	N	L^1 error	order	L^∞ error	order	L^2 error	order
$a_1(x) = 0.54 \cdot g'(u_x^n)$	128	NaN		NaN		NaN	
	256	NaN	NaN	NaN	NaN	NaN	NaN
	512	NaN	NaN	NaN	NaN	NaN	NaN
	1024	NaN	NaN	NaN	NaN	NaN	NaN
	2048	NaN	NaN	NaN	NaN	NaN	NaN
$a_1(x) = g'(u_x^n)$	128	NaN		NaN		NaN	
	256	2.83E-05	NaN	1.58E-04	NaN	4.27E-05	NaN
	512	4.48E-06	2.66	3.27E-05	2.27	7.53E-06	2.50
	1024	8.92E-07	2.33	5.89E-06	2.47	1.39E-06	2.43
	2048	1.58E-07	2.50	9.59E-07	2.62	2.32E-07	2.59
$\tilde{a}_1(x) = 0.54 \cdot \tilde{g}(x)$	128	1.44E-04		7.34E-04		2.21E-04	
	256	4.96E-05	1.54	2.18E-04	1.75	7.32E-05	1.59
	512	1.18E-05	2.07	4.79E-05	2.19	1.61E-05	2.19
	1024	1.46E-06	3.01	4.98E-06	3.27	1.85E-06	3.12
	2048	8.20E-08	4.16	5.80E-07	3.10	1.24E-07	3.90
$\tilde{a}_1(x) = \tilde{g}(x)$	128	3.58E-04		1.98E-03		5.94E-04	
	256	1.73E-04	1.05	8.99E-04	1.14	2.72E-04	1.13
	512	6.18E-05	1.48	2.57E-04	1.81	9.03E-05	1.59
	1024	1.30E-05	2.25	5.30E-05	2.28	1.81E-05	2.32
	2048	1.25E-06	3.37	5.18E-06	3.35	1.69E-06	3.43

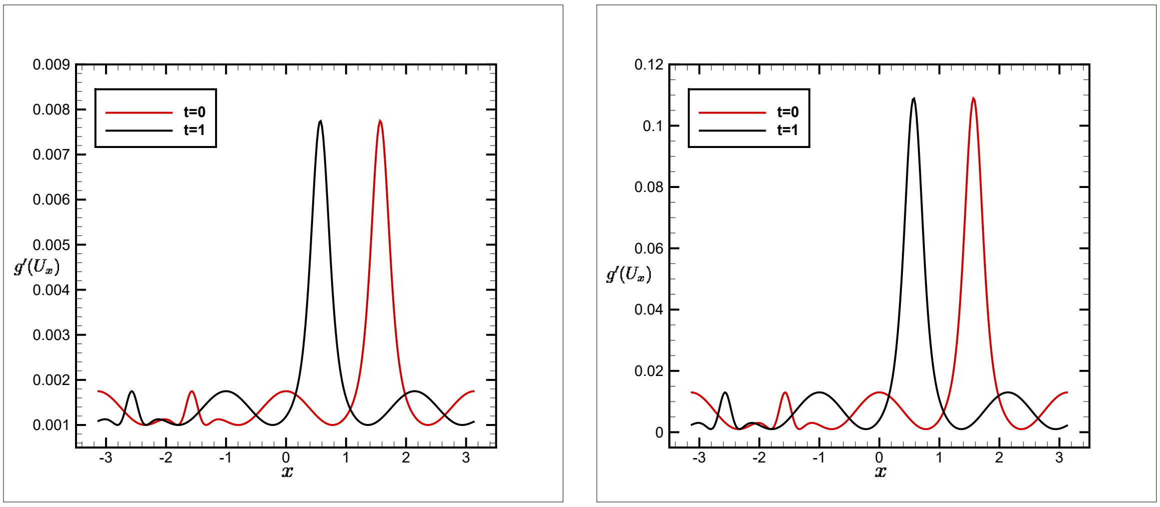

Figure 3.4: *Snapshots of $g'(U_x)$ at the indicated times. Left:* $\alpha = 0.001$, $\beta = 0.025$, $\gamma = -0.05$, $\lambda = 0.05$, $\sigma = 4$, $\eta = 2$. *Right:* $\alpha = 0.001$, $\beta = 0.1$, $\gamma = -0.1$, $\lambda = 0.1$, $\sigma = 4$, $\eta = 2$.

Table 3.12: The errors and orders of the VC-EIN-LDG and CC-EIN-LDG schemes for Example (3.9) with $\alpha = 0.001$, $\beta = 0.025$, $\gamma = -0.05$, $\lambda = 0.05$, $\sigma = 4$, $\eta = 2$.

VC-EIN-LDG							
$\tilde{a}_1(x)$	N	L^1 error	order	L^∞ error	order	L^2 error	order
$0.54 \cdot \tilde{g}(x)$	256	1.07E-06		5.74E-06		1.58E-06	
	512	2.33E-07	2.20	9.62E-07	2.58	3.37E-07	2.23
	1024	3.60E-08	2.70	1.41E-07	2.77	4.94E-08	2.77
	2048	4.71E-09	2.93	1.89E-08	2.90	6.32E-09	2.97
	4096	5.95E-10	2.98	2.46E-09	2.94	7.95E-10	2.99
CC-EIN-LDG							
b_1	N	L^1 error	order	L^∞ error	order	L^2 error	order
$0.54 \cdot \max g'(u_x^n)$	256	1.27E-06		8.09E-06		1.95E-06	
	512	5.09E-07	1.32	1.99E-06	2.03	6.93E-07	1.49
	1024	9.76E-08	2.38	4.13E-07	2.27	1.36E-07	2.35
	2048	1.24E-08	2.97	5.57E-08	2.89	1.75E-08	2.96
	4096	1.53E-09	3.02	7.05E-09	2.98	2.16E-09	3.01

Table 3.13: The errors and orders of the VC-EIN-LDG and CC-EIN-LDG schemes for Example (3.9) with $\alpha = 0.001$, $\beta = 0.1$, $\gamma = -0.1$, $\lambda = 0.1$, $\sigma = 4$, $\eta = 2$.

VC-EIN-LDG							
$\tilde{a}_1(x)$	N	L^1 error	order	L^∞ error	order	L^2 error	order
$0.54 \cdot \tilde{g}(x)$	256	2.20E-04		1.69E-03		3.70E-04	
	512	1.16E-04	0.92	7.83E-04	1.11	1.92E-04	0.95
	1024	4.30E-05	1.43	2.40E-04	1.70	6.51E-05	1.56
	2048	7.16E-06	2.59	3.14E-05	2.94	9.67E-06	2.75
	4096	5.38E-07	3.74	2.38E-06	3.72	6.91E-07	3.81
CC-EIN-LDG							
b_1	N	L^1 error	order	L^∞ error	order	L^2 error	order
$0.54 \cdot \max g'(u_x^n)$	256	3.30E-04		1.82E-03		4.67E-04	
	512	1.40E-04	1.24	8.87E-04	1.04	2.12E-04	1.14
	1024	5.46E-05	1.36	3.75E-04	1.24	8.52E-05	1.31
	2048	2.00E-05	1.45	1.30E-04	1.52	3.13E-05	1.44
	4096	5.19E-06	1.94	2.88E-05	2.18	8.29E-06	1.92

augmented with the exact solution

$$U(x,t) = \sin(x + \lambda t). \tag{3.11}$$

The initial solution is extracted from the exact solution and the source term $s(x,t)$ is chosen properly such that the exact solution satisfies the given equation.

First, we numerically validate the stability and error accuracy of the VC-EIN-LDG scheme. In the test, we take the parameters $\alpha = 0$, $\beta = 6$, $\lambda = \frac{1}{3}$. The numerical results of the scheme with $a_1(x) = 1000 \cdot g'(u_x^n)$ and $\tilde{a}_1(x) = 0.54 \cdot \tilde{g}(x)$ at time $T = 1$ are presented in Table 3.14. Note that for the VC-EIN-LDG scheme, the dilation parameters are set as $C_0 = 1.6$, $\delta = 0.9$ and remain unchanged in the test. As expected, the scheme is stable for $\tilde{a}_1(x) = 0.54 \cdot \tilde{g}(x)$. Even though we greatly increase the value of a_0 to 1000, $a_1(x) = a_0 \cdot d(u^n)$ still cannot ensure the stability of the scheme. Second, the CC-EIN-LDG scheme is also used to solve the nonlinear problem. In the test, we take $b_1 = 0.54 \cdot \max g'(u_x^n)$. The numerical results of the scheme are also listed in Table 3.14, from which we can see that the CC-EIN-LDG scheme is stable as always and the numerical orders of accuracy settle down towards the asymptotic value slowly with mesh refinements. Similarly, due to the fact the errors are larger near the bumps and such errors do not decrease much from the CC-EIN method to the VC-EIN method, the global errors of the VC-EIN-LDG scheme are comparable with the CC-EIN-LDG scheme. However, in regions away from the bumps, namely $[0,1] \cup [5, 2\pi]$, the VC-EIN method produces much smaller errors than the CC-EIN method, as can be seen in Table 3.15.

3.2.4 The nonlinear numerical test in two dimensions

We consider the two-dimensional nonlinear dispersion equation

$$U_t + g(U_y)_{xy} = s(x,y,t), \qquad (x,y) \in (-\pi,\pi)^2 \tag{3.12}$$

augmented with the dispersion coefficient

$$g(U_y) = \alpha U_y + \beta U_y^3$$

Table 3.14: The errors and orders of the VC-EIN-LDG and CC-EIN-LDG schemes for Example (3.10) with $\alpha = 0$, $\beta = 6$, $\lambda = \frac{1}{3}$ in $[0, 2\pi]$.

VC-EIN-LDG							
	N	L^1 error	order	L^∞ error	order	L^2 error	order
$a_1(x) = 1000 \cdot g'(u_x^n)$	128	NaN		NaN		NaN	
	256	NaN	NaN	NaN	NaN	NaN	NaN
	512	NaN	NaN	NaN	NaN	NaN	NaN
	1024	NaN	NaN	NaN	NaN	NaN	NaN
	2048	NaN	NaN	NaN	NaN	NaN	NaN
$\tilde{a}_1(x) = 0.54 \cdot \tilde{g}(x)$	128	3.26E-04		2.91E-03		6.09E-04	
	256	1.40E-04	1.21	1.64E-03	0.82	3.05E-04	1.00
	512	4.08E-05	1.78	5.32E-04	1.63	9.55E-05	1.67
	1024	8.98E-06	2.18	1.15E-04	2.21	2.24E-05	2.09
	2048	1.72E-06	2.39	2.87E-05	2.01	4.99E-06	2.17

CC-EIN-LDG							
b_1	N	L^1 error	order	L^∞ error	order	L^2 error	order
$0.54 \cdot \max g'(u_x^n)$	128	6.39E-05		2.61E-04		9.50E-05	
	256	1.63E-05	1.97	7.78E-05	1.75	2.44E-05	1.96
	512	3.70E-06	2.14	2.11E-05	1.88	5.84E-06	2.06
	1024	8.22E-07	2.17	5.82E-06	1.86	1.44E-06	2.02
	2048	1.79E-07	2.20	1.63E-06	1.83	3.49E-07	2.04

Table 3.15: The errors and orders of the VC-EIN-LDG and CC-EIN-LDG schemes for Example (3.10) with $\alpha = 0$, $\beta = 6$, $\lambda = \frac{1}{3}$ in $[0,1] \cup [5, 2\pi]$.

VC-EIN-LDG							
$\tilde{a}_1(x)$	N	L^1 error	order	L^∞ error	order	L^2 error	order
$0.54 \cdot \tilde{g}(x)$	128	3.37E-09		6.05E-09		3.81E-09	
	256	4.11E-10	3.04	6.07E-10	3.32	4.62E-10	3.05
	512	5.07E-11	3.02	7.18E-11	3.08	5.52E-11	3.06
	1024	5.91E-12	3.10	8.83E-12	3.02	6.81E-12	3.02
	2048	7.13E-13	3.05	1.06E-12	3.06	8.17E-13	3.06
CC-EIN-LDG							
b_1	N	L^1 error	order	L^∞ error	order	L^2 error	order
$0.54 \cdot \max g'(u_x^n)$	128	6.27E-05		2.28E-04		8.10E-05	
	256	1.26E-05	2.31	3.84E-05	2.57	1.74E-05	2.22
	512	2.20E-06	2.52	1.22E-05	1.66	3.60E-06	2.27
	1024	2.47E-07	3.16	1.20E-06	3.34	4.29E-07	3.07
	2048	2.89E-08	3.10	2.60E-07	2.21	5.38E-08	2.99

and the exact solution

$$U(x,y,t) = \gamma \sin(\eta(x+y+t)) - \lambda \tanh(\sigma \cos(x+y+t)).$$

The initial solution is extracted from the exact solution and the source term $s(x,y,t)$ is chosen properly such that the exact solution satisfies the given equation.

First, we numerically validate the stability and order of accuracy of the VC-EIN-LDG scheme. In the test, we take the parameters $\alpha = 0.001$, $\beta = 0.02$, $\gamma = -0.05$, $\lambda = 0.05$, $\sigma = 2$, $\eta = 2$. The numerical results of the VC-EIN-LDG scheme with $a_1(x,y) = 0.54 \cdot g'(u_y^n)$ and $\tilde{a}_1(x,y) = 0.54 \cdot \tilde{g}(x,y)$ at time $T = 1$ are presented in Table 3.16. Note that in the test the dilation parameters are always taken as $C_0 = 1.6$ and $\delta = 0.7$. It is observed that the scheme is stable for $\tilde{a}_1(x,y) = 0.54 \cdot \tilde{g}(x,y)$ and can achieve very nice third order convergence rates for L^1, L^2 and L^∞ norms. Second, the CC-EIN-LDG scheme is also used to solve the nonlinear problem. In the test, we take $b_1 = 0.54 \cdot \max g'(u_y^n)$. The numerical results of the scheme are also listed in Table 3.16, from which we can see that the CC-EIN-LDG scheme is stable as always. Under the same mesh grid, the results of the VC-EIN-LDG scheme are compared against those of the CC-EIN-LDG scheme. In this case, the global errors of the VC-EIN-LDG scheme are comparable with the CC-EIN-LDG scheme.

Table 3.16: The errors and orders of the VC-EIN-LDG and CC-EIN-LDG schemes for Example (3.12) with $\alpha = 0.001$, $\beta = 0.02$, $\gamma = -0.05$, $\lambda = 0.05$, $\sigma = 2$, $\eta = 2$.

VC-EIN-LDG

	N	L^1 error	order	L^∞ error	order	L^2 error	order
$a_1(x,y) = 0.54 \cdot g'(u_y^n)$	20	NaN		NaN		NaN	
	40	NaN	NaN	NaN	NaN	NaN	NaN
	60	NaN	NaN	NaN	NaN	NaN	NaN
	80	NaN	NaN	NaN	NaN	NaN	NaN
	100	NaN	NaN	NaN	NaN	NaN	NaN
$\tilde{a}_1(x,y) = 0.54 \cdot \tilde{g}(x,y)$	20	2.45E-04		1.38E-03		3.29E-04	
	40	3.13E-05	2.97	2.48E-04	2.48	4.32E-05	2.93
	60	8.84E-06	3.12	8.26E-05	2.71	1.27E-05	3.01
	80	3.83E-06	2.91	3.73E-05	2.77	5.58E-06	2.87
	100	1.99E-06	2.93	1.97E-05	2.86	2.92E-06	2.90

CC-EIN-LDG

	N	L^1 error	order	L^∞ error	order	L^2 error	order
$b_1 = 0.54 \cdot \max g'(u_y^n)$	20	2.42E-04		1.46E-03		3.29E-04	
	40	3.10E-05	2.96	2.51E-04	2.54	4.31E-05	2.93
	60	8.77E-06	3.12	8.25E-05	2.74	1.27E-05	3.00
	80	3.79E-06	2.92	3.70E-05	2.79	5.58E-06	2.87
	100	1.98E-06	2.92	1.95E-05	2.88	2.92E-06	2.90

3.3 The fourth order diffusion equations

In this subsection, we would like to test the performance and stability of the proposed schemes for the fourth order diffusion equation (1.3). As a dissipative equation, it has many similarities in properties with the second order diffusion equation (1.1). To save space, we only take the fourth order diffusion equation in one dimension as an example to present the results.

3.3.1 The nonlinear numerical test in one dimension

We consider the fourth order diffusion equation

$$U_t + (d(U_x)U_{xx})_{xx} = s(x,t), \qquad x \in (-\pi, \pi) \tag{3.13}$$

augmented with the coefficient

$$d(U_x) = (\gamma + \alpha e^{-\sigma^2(1-U_x)})(2U_x^2 - 1)^2$$

and periodic boundary conditions. The exact solution is given by (3.11). The initial solution is extracted from the exact solution and the source term $s(x,t)$ is chosen properly such that the exact solution satisfies the given equation.

Similarly, for such a nonlinear problem, since the stability condition (2.19) involves the unknown solutions above the n-th time level, the VC-EIN-LDG scheme is adjusted for use with the help of the convolution technique. In short, we add and subtract a fourth derivative term with variable coefficient $(\tilde{a}_1(x)U_{xx})_{xx}$ at the left-hand side of the equation

$$U_t + \underbrace{(d(U_x)U_{xx} - \tilde{a}_1(x)U_{xx})_{xx} - s(x,t)}_{T_1} + \underbrace{(\tilde{a}_1(x)U_{xx})_{xx}}_{T_2} = 0,$$

where $\tilde{a}_1(x) = a_0 \cdot \hat{d}(x)$ and $\hat{d}(x)$ is the convolution of $d(u_x^n)$ and the dilated mollifier $\Phi_{C_0,\delta}(x)$ defined by (2.20). By adjusting the dilation parameters δ and C_0, we can always make the inequality (2.23) tenable to ensure the stability of the VC-EIN-LDG scheme. Again, the adjustment strategy of the dilation parameters δ and C_0 is similar to that described in Section 2.3 for the second order diffusion equations.

First, we numerically validate the stability of the VC-EIN-LDG scheme. In the test, we take the parameters $\gamma = 0$, $\alpha = 20$, $\sigma = 3$, $\lambda = \frac{1}{10}$. With those parameters, the diffusion coefficient $d(U_x)$, for any time $t \geq 0$, forms a steep bump with the value of $d(U_x)$ outside the bump decaying exponentially. The numerical results of the scheme with $a_1(x) = 100 \cdot d(u_x^n)$ and $\tilde{a}_1(x) = 0.54 \cdot \hat{d}(x)$ are presented in Table 3.17. Note that for the VC-EIN-LDG scheme, the dilation parameters are set as $C_0 = 1.7$ and $\delta = 0.7$ and remain unchanged in the test.

As expected, the scheme is stable for $\tilde{a}_1(x) = 0.54 \cdot \hat{d}(x)$. Second, the CC-EIN-LDG scheme is also used to solve the nonlinear problem. In the test, we take $b_1 = 0.54 \cdot \max d(u_x^n)$. The numerical results of the scheme are also listed in Table 3.17, from which we can see that the CC-EIN-LDG scheme is stable as always and the numerical orders of accuracy settle down towards the asymptotic value slowly with mesh refinements. Due to the fact the errors are larger near the bumps and such errors do not decrease much from the CC-EIN method to the VC-EIN method, the global errors of the VC-EIN-LDG scheme are comparable with the CC-EIN-LDG scheme. However, in regions away from the bumps, namely $x \in [-\pi, 2.5] \cup [2.5, \pi]$, the VC-EIN method produces much smaller errors than the CC-EIN method, as can be seen in Table 3.18.

Table 3.17: The errors and orders of the VC-EIN-LDG and CC-EIN-LDG schemes for Example (3.13) with $\gamma = 0$, $\alpha = 20$, $\sigma = 3$, $\lambda = \frac{1}{10}$ in $[-\pi, \pi]$.

VC-EIN-LDG							
$\tilde{a}_1(x)$	N	L^1 error	order	L^∞ error	order	L^2 error	order
$100 \cdot d(u_x^n)$	40	1.71E-02		4.75E-02		2.36E-02	
	80	NaN	NaN	NaN	NaN	NaN	NaN
	160	NaN	NaN	NaN	NaN	NaN	NaN
	320	NaN	NaN	NaN	NaN	NaN	NaN
	640	NaN	NaN	NaN	NaN	NaN	NaN
$0.54 \cdot \hat{d}(x)$	40	6.62E-03		1.52E-02		8.76E-03	
	80	3.87E-03	0.77	7.96E-03	0.93	5.09E-03	0.78
	160	2.05E-03	0.92	4.23E-03	0.91	2.68E-03	0.92
	320	9.79E-04	1.07	2.08E-03	1.03	1.28E-03	1.07
	640	4.02E-04	1.28	8.83E-04	1.23	5.24E-04	1.29
CC-EIN-LDG							
b_1	N	L^1 error	order	L^∞ error	order	L^2 error	order
$0.54 \cdot \max d(u_x^n)$	40	6.13E-03		9.76E-03		6.75E-03	
	80	1.68E-03	1.86	2.69E-03	1.86	1.85E-03	1.87
	160	3.50E-04	2.27	5.56E-04	2.27	3.84E-04	2.27
	320	6.02E-05	2.54	9.00E-05	2.63	6.56E-05	2.55
	640	1.22E-05	2.31	2.79E-05	1.69	1.38E-05	2.25

Table 3.18: The errors and orders of the VC-EIN-LDG and CC-EIN-LDG schemes for Example (3.13) with $\gamma = 0$, $\alpha = 20$, $\sigma = 3$, $\lambda = \frac{1}{10}$ in $[-\pi, -2.5] \cup [2.5, \pi]$.

VC-EIN-LDG

$\tilde{a}_1(x)$	N	L^1 error	order	L^∞ error	order	L^2 error	order
$0.54 \cdot \hat{d}(x)$	40	1.08E-05		1.55E-05		1.12E-05	
	80	1.25E-06	3.10	2.02E-06	2.95	1.42E-06	2.98
	160	1.64E-07	2.93	6.73E-07	1.58	1.92E-07	2.89
	320	2.21E-08	2.89	1.63E-07	2.04	2.84E-08	2.76
	640	2.70E-09	3.04	1.56E-08	3.38	3.28E-09	3.11

CC-EIN-LDG

b_1	N	L^1 error	order	L^∞ error	order	L^2 error	order
$0.54 \cdot \max d(u_x^n)$	40	9.11E-03		9.76E-03		9.13E-03	
	80	2.49E-03	1.87	2.69E-03	1.86	2.50E-03	1.87
	160	5.19E-04	2.27	5.56E-04	2.27	5.20E-04	2.27
	320	8.49E-05	2.61	9.00E-05	2.63	8.50E-05	2.61
	640	1.10E-05	2.95	1.37E-05	2.72	1.11E-05	2.94

4 Concluding remarks

The present study investigates the stability and performance of a third order VC-EIN method in conjunction with the LDG methods for the high order diffusion and dispersion equations, respectively. Unlike the CC-EIN method, the auxiliary term we add to and subtract from the original equation is a spatially varying linear term. Based on the stability results of the schemes for simplified linear equations [14], we provide a guidance for the choice of the variable coefficient $a_1(x)$ to ensure the stability of the VC-EIN-LDG scheme for the quasi-linear and nonlinear equations. Numerical experiments show that the schemes can be stable under a relatively coarse mesh grid and achieve optimal orders of accuracy when the stability constraints (2.17), (2.18) and (2.19) are satisfied. As a comparative study we also revisit the CC-EIN-LDG scheme studied in [14]. When proper parameters δ, C_0, a_0 are chosen, the numerical results show that the VC-EIN-LDG scheme is more accurate than the CC-EIN-LDG scheme of the same order, if the diffusion coefficient or the dispersion coefficient has a few high and narrow bumps and the bumps only account for a small part of the whole computational domain. We have only considered one and two dimensional problems in this paper. The method can be applied to three dimensions in the same fashion, which will be carried out in our future work.

References

[1] U. M. Ascher, S. J. Ruuth and R. J. Spiteri, *Implicit-explicit Runge-Kutta methods for time-dependent partial differential equations*, Applied Numerical Mathematics, 25, 1997, 151-167.

[2] F. Bassi, L. Botti, A. Colombo, A. Ghidoni and F. Massa, *Linearly implicit Rosenbrock-type Runge-Kutta schemes applied to the Discontinuous Galerkin solution of compressible and incompressible unsteady flows*, Computers and Fluids, 118, 2015, 305-320.

[3] T. B. Benjamin, J. L. Bona and J. J. Mahony, *Model equations for long waves in nonlinear dispersive systems*, Philosophical Transactions of the Royal Society A: Mathematical Physical and Engineering Sciences, 272, 1972, 47-78.

[4] S. Boscarino, P.-G. LeFloch and G. Russo, *On a class of uniformly accurate IMEX Runge-Kutta schemes and application to hyperbolic systems with relaxation*, SIAM Journal on Scientific Computing, 36, 2014, 377-395.

[5] P. Cavaliere, G. Zavarise and M. Perillo, *Modeling of the carburizing and nitriding processes*, Computational Materials Science, 46, 2009, 26-35.

[6] B. Cockburn and C.-W. Shu, *The local discontinuous Galerkin method for time-dependent convection-diffusion systems*, SIAM Journal on Numerical Analysis, 35, 1998, 2440-2463.

[7] B. Cockburn and C.-W. Shu, *Runge-Kutta discontinuous Galerkin methods for convection-dominated problems*, Journal of Scientific Computing, 16, 2001, 173-261.

[8] J. Douglas Jr and T. Dupont, *Alternating-direction Galerkin methods on rectangles*, Numerical Solution of Partial Differential Equations-II, New York: Academic Press, 1971, 133-214.

[9] L. Duchemin and J. Eggers, *The explicit-implicit-null method: Removing the numerical instability of PDEs*, Journal of Computational Physics, 263, 2014, 37-52.

[10] F. Filbet and S. Jin, *A class of asymptotic-preserving schemes for kinetic equations and related problems with stiff sources*, Journal of Computational Physics, 229, 2010, 7625-7648.

[11] F. X. Giraldo, J. F. Kelly and E. M. Constantinescu, *Implicit-Explicit formulations of a three-dimensional nonhydrostatic unified model of the atmosphere (NUMA)*, SIAM Journal on Scientific Computing, 35, 2013, B1162-B1194.

[12] H. Shi and Y. Li, *Local discontinuous Galerkin methods with implicit-explicit multistep time-marching for solving the nonlinear Cahn-Hilliard equation*, Journal of Computational Physics, 394, 2019, 719-731.

[13] P. Smereka, *Semi-Implicit level set methods for curvature and surface diffusion motion*, Journal of Scientific Computing, 19, 2003, 439-456.

[14] M. Tan, J. Cheng and C.-W. Shu, *Stability of high order finite difference and local discontinuous Galerkin schemes with explicit-implicit-null time-marching for high order dissipative and dispersive equations*, Journal of Computational Physics, 464, 2022, 111314.

[15] M. Tan, J. Cheng and C.-W. Shu, *Stability of spectral collocation schemes with explicit-implicit-null time-marching for convection-diffusion and convection-dispersion equations*, East Asian Journal on Applied Mathematics, 13, 2023, 464-498.

[16] H. Wang, Q. Zhang, S. Wang and C.-W. Shu, *Local discontinuous Galerkin methods with explicit-implicit-null time discretizations for solving nonlinear diffusion problems*, Science China Mathematics, 63, 2020, 183-204.

[17] Y. Xu and C.-W. Shu, *Optimal error estimates of the semidiscrete local discontinuous Galerkin methods for high order wave equations*, SIAM Journal on Numerical Analysis, 50, 2012, 79-104.

[18] Y. Xu and C.-W. Shu, *Local discontinuous Galerkin methods for three classes of nonlinear wave equations*, Journal of Computational Mathematics, 22, 2004, 250-274.

[19] J. Yan and C.-W. Shu, *A local discontinuous Galerkin method for KdV type equations*, SIAM Journal on Numerical Analysis, 40, 2002, 769-791.

[20] J. Yan and C.-W. Shu, *A Local discontinuous Galerkin methods for partial differential equations with higher order derivatives*, Journal of Scientific Computing, 17, 2002, 27-47.

[21] Q. Zhang and Z. Wu, *Numerical simulation for porous medium equation by local discontinuous Galerkin finite element method*, Journal of Scientific Computing, 38, 2009, 127-148.

Appendix

A.1 Stability analysis of the LDG method (2.2)

Theorem 1: *The numerical scheme* (2.2) *with the choice of fluxes* (2.6) *is L^2 stable, i.e.*

$$\frac{1}{2}\frac{\mathrm{d}}{\mathrm{d}t}\int_\Omega u^2\,\mathrm{d}x + \int_\Omega d(u) r^2\,\mathrm{d}x \leq 0. \tag{A.1}$$

Proof. We sum up the four equalities in (2.2) and introduce the notation

$$\begin{aligned} B_j(u,p,q,r;\,\phi_1,\phi_2,\phi_3,\phi_4) = &\int_{I_j} u_t\phi_1\,\mathrm{d}x + \int_{I_j}(p+q)(\phi_1)_x\,\mathrm{d}x - (\hat{p}+\hat{q})_{j+\frac{1}{2}}(\phi_1)^-_{j+\frac{1}{2}} \\ &+ (\hat{p}+\hat{q})_{j-\frac{1}{2}}(\phi_1)^+_{j-\frac{1}{2}} + \int_{I_j} p\phi_2\,\mathrm{d}x - \int_{I_j}(d(u)-a_1(x))r\phi_2\,\mathrm{d}x \\ &+ \int_{I_j} q\phi_3\,\mathrm{d}x - \int_{I_j} a_1(x) r\phi_2\,\mathrm{d}x + \\ &\int_{I_j} r\phi_4\,\mathrm{d}x + \int_{I_j} u(\phi_4)_x\,\mathrm{d}x - \hat{u}_{j+\frac{1}{2}}(\phi_4)^-_{j+\frac{1}{2}} + \hat{u}_{j-\frac{1}{2}}(\phi_4)^+_{j-\frac{1}{2}}. \end{aligned}$$

Obviously, the solutions u, p, q, r of the scheme satisfy

$$B_j(u,p,q,r;\,\phi_1,\phi_2,\phi_3,\phi_4) = 0$$

for all ϕ_1, ϕ_2, ϕ_3, $\phi_4 \in V_h$. We then take

$$\phi_1 = u, \qquad \phi_2 = -r, \qquad \phi_3 = -r, \qquad \phi_4 = p+q$$

to obtain, after some algebraic manipulations,

$$0 = B_j(u,p,q,r;\,u,-r,-r,p+q) = \frac{1}{2}\frac{\mathrm{d}}{\mathrm{d}t}\int_{I_j} u^2\,\mathrm{d}x + \int_{I_j} d(u)r^2\,\mathrm{d}x + (\hat{H}_{j+\frac{1}{2}} - \hat{H}_{j-\frac{1}{2}}) + \Theta_{j-\frac{1}{2}},$$

where

$$\begin{aligned} \hat{H} &= \big(u(p+q)\big)^- - (\hat{p}+\hat{q})u^- - \hat{u}(p+q)^-, \\ \Theta &= -[u(p+q)] + (\hat{p}+\hat{q})[u] + \hat{u}[(p+q)]. \end{aligned}$$

Here, $[u]$ denotes $u^+ - u^-$. To this end, we notice that, with the definition of the numerical fluxes (2.6) and periodic boundary condition, we can easily obtain $\Theta_{j-\frac{1}{2}} = 0$. Then we sum over j to obtain (A.1). □

A.2 Stability analysis of the LDG method (2.12)

Theorem 1: *The numerical scheme* (2.12) *with the choice of fluxes* (2.13) *is L^2 stable, i.e.*

$$\frac{1}{2}\frac{\mathrm{d}}{\mathrm{d}t}\int_\Omega u^2\,\mathrm{d}x + \int_\Omega d(v)w^2\,\mathrm{d}x \le 0. \tag{A.2}$$

Proof. We sum up the equalities in (2.12) and introduce the notation

$$\begin{aligned}
B_j(u,r,z,p,q,w,v;\,\phi_l) = {} & \int_{I_j} u_t\phi_1\,\mathrm{d}x - \int_{I_j}(r+z)(\phi_1)_x\,\mathrm{d}x + (\hat{r}+\hat{z})_{j+\frac{1}{2}}(\phi_1)^-_{j+\frac{1}{2}} - (\hat{r}+\hat{z})_{j-\frac{1}{2}}(\phi_1)^+_{j-\frac{1}{2}} \\
& + \int_{I_j} r\phi_2\,\mathrm{d}x + \int_{I_j} p(\phi_2)_x\,\mathrm{d}x - \hat{p}_{j+\frac{1}{2}}(\phi_2)^-_{j+\frac{1}{2}} + \hat{p}_{j-\frac{1}{2}}(\phi_2)^+_{j-\frac{1}{2}} \\
& + \int_{I_j} z\phi_3\,\mathrm{d}x + \int_{I_j} q(\phi_3)_x\,\mathrm{d}x - \hat{q}_{j+\frac{1}{2}}(\phi_3)^-_{j+\frac{1}{2}} + \hat{q}_{j-\frac{1}{2}}(\phi_3)^+_{j-\frac{1}{2}} \\
& + \int_{I_j} p\phi_4\,\mathrm{d}x - \int_{I_j}(d(v)-a_1(x))w\phi_4\,\mathrm{d}x \\
& + \int_{I_j} q\phi_5\,\mathrm{d}x - \int_{I_j} a_1(x)w\phi_5\,\mathrm{d}x \\
& + \int_{I_j} w\phi_6\,\mathrm{d}x + \int_{I_j} v(\phi_6)_x\,\mathrm{d}x - \hat{v}_{j+\frac{1}{2}}(\phi_6)^-_{j+\frac{1}{2}} + \hat{v}_{j-\frac{1}{2}}(\phi_6)^+_{j-\frac{1}{2}} \\
& + \int_{I_j} v\phi_7\,\mathrm{d}x + \int_{I_j} u(\phi_7)_x\,\mathrm{d}x - \hat{u}_{j+\frac{1}{2}}(\phi_7)^-_{j+\frac{1}{2}} + \hat{u}_{j-\frac{1}{2}}(\phi_7)^+_{j-\frac{1}{2}}.
\end{aligned}$$

Obviously, the solutions u, r, z, p, q, w, v of the scheme satisfy

$$B_j(u,r,z,p,q,w,v;\,\phi_l) = 0$$

for all $\phi_l \in V_h$, $1 \le l \le 7$. We then take

$$\phi_1 = u, \qquad \phi_2 = \phi_3 = v, \qquad \phi_4 = \phi_5 = -w, \qquad \phi_6 = p+q, \qquad \phi_7 = -(r+z)$$

to obtain, after some algebraic manipulations,

$$0 = B_j = \frac{1}{2}\frac{\mathrm{d}}{\mathrm{d}t}\int_{I_j} u^2\,\mathrm{d}x + \int_{I_j} d(v)w^2\,\mathrm{d}x + (\hat{H}_{j+\frac{1}{2}} - \hat{H}_{j-\frac{1}{2}}) + \Theta_{j-\frac{1}{2}},$$

where

$$\begin{aligned}
\hat{H} &= -\big(u(r+z)\big)^- + \big(v(p+q)\big)^- + (\hat{r}+\hat{z})u^- - (\hat{p}+\hat{q})v^- - \hat{v}(p+q)^- + \hat{u}(r+z)^-, \\
\Theta &= [u(r+z)] - [v(p+q)] - (\hat{r}+\hat{z})[u] + (\hat{p}+\hat{q})[v] + \hat{v}[p+q] - \hat{u}[r+z].
\end{aligned}$$

Here, $[u]$ denotes $u^{+} - u^{-}$. To this end, we notice that, with the definition of the numerical fluxes (2.13) and periodic boundary condition, we can easily obtain $\Theta_{j-\frac{1}{2}} = 0$. Then we sum over j to obtain (A.2). □